

# MMEarth-Bench: Global Model Adaptation via Multimodal Test-Time Training

Lucia Gordon<sup>1,2\*</sup>Serge Belongie<sup>2</sup>Christian Igel<sup>2</sup>Nico Lang<sup>2</sup><sup>1</sup>Harvard University, USA    <sup>2</sup>University of Copenhagen, Denmark

## Abstract

Recent research in geospatial machine learning has demonstrated that models pretrained with self-supervised learning on Earth observation data can perform well on downstream tasks with limited training data. However, most of the existing geospatial benchmark datasets have few data modalities and poor global representation, limiting the ability to evaluate multimodal pretrained models at global scales. To fill this gap, we introduce MMEARTH-BENCH, a collection of five new multimodal environmental tasks with 12 modalities, globally distributed data, and both in- and out-of-distribution test splits. We benchmark a diverse set of pretrained models and find that while (multimodal) pretraining tends to improve model robustness in limited data settings, geographic generalization abilities remain poor. In order to facilitate model adaptation to new downstream tasks and geographic domains, we propose a model-agnostic method for test-time training with multimodal reconstruction (TTT-MMR) that uses all the modalities available at test time as auxiliary tasks, regardless of whether a pretrained model accepts them as input. Our method improves model performance on both the random and geographic test splits, and geographic batching leads to a good trade-off between regularization and specialization during TTT. Our dataset, code, and visualization tool are linked from the project page at [lgordon99.github.io/mmearth-bench](https://lgordon99.github.io/mmearth-bench).

## 1. Introduction

Earth observation (EO) data helps us monitor our planet's health, respond to natural disasters, and tackle societal challenges such as the Sustainable Development Goals (SDGs) [45]. A multitude of sensors provide unprecedented data about the planet but also far exceed what most data processing pipelines can handle. To realize the potential of EO data, raw observations, such as optical satellite images, must be interpreted at global scales. Deep learning seems like a natural approach to analyzing copious unlabeled data, and supervised learning has shown great success

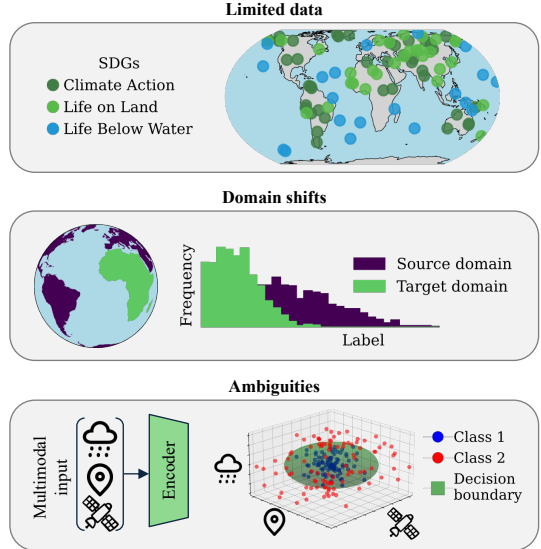


Figure 1. **Self-supervised multimodal pretraining promises to overcome the grand challenges in Earth observation.** Crucial applications have to rely on *limited and sparse* and *geographically biased* training data. Furthermore, the *ambiguities* inherent to modeling biophysical quantities with remotely sensed data may be resolved by models conditioned on *multiple modalities*.

in the case of abundant reference data [75], but we identify *three grand challenges* yet to be overcome (see Fig. 1). The first long-standing challenge has been the sparsity and limited amount of labeled data, as is often the case in crucial applications where reference data is collected through field measurements [75]. The second challenge is geographic generalization, *i.e.* the domain shift that occurs when using a model trained on one geographic region to make predictions on another [37]. Lastly, the third main challenge is to minimize the ambiguities inherent to estimating biophysical quantities from observational, especially unimodal, EO data [50]. The research community working at the intersection of machine learning and EO has identified self-supervised learning (SSL) as a promising way forward [3, 28, 42, 61]. Pretraining models with global unlabeled data promises to facilitate model adaptation to tasks with limited labeled data and ameliorate performance drops

\*Correspondence: [lgordon@cs.harvard.edu](mailto:lgordon@cs.harvard.edu)

in geographic regions without reference data. Because EO data is georeferenced, the multitude of sensors and satellites means that there are myriad data modalities that can be automatically aligned [42]. This represents an opportunity for multimodal data fusion to resolve ambiguities in model predictions [46, 52, 55, 60]. Hence, EO is relevant to the computer vision community for advancing multimodal representation learning [40]. While existing EO benchmarks [10, 22, 30, 37, 63] have helped to develop and evaluate pretrained EO models, they limit the evaluation of progress towards overcoming these three grand challenges, as most of their downstream tasks are i) regional rather than global, ii) not evaluated on geographic splits with an entire held-out region, and iii) only provide few modalities per task.

In this work, we introduce MMEARTH-BENCH, a multimodal EO benchmark dataset containing five global tasks designed to evaluate pretrained EO models in these three challenging yet crucial settings. We evaluate a diverse set of pretrained models on our benchmark. As is the case with our evaluation and more generally, there is a mismatch between the *input modalities* on which a model was pretrained and the *task modalities* available at inference time [37]. The standard practice is simply to use only the task modalities that the pretrained model can take as input. To address this inefficiency, we introduce a method for *using all available modalities at test time, whether or not they are compatible with the pretrained model*. Complementary to using multimodal data for self-supervised pretraining, we propose using the modalities as reconstruction tasks in the regime of test-time adaptation, which uses unlabeled test data to adapt the encoder at test time. We formulate our proposed method for Test-Time Training with MultiModal Reconstruction (TTT-MMR), along with a second variant using geographic batching (TTT-MMR-GEO), and show that this leads to a good trade-off between specialization and regularization, a crucial aspect in TTT [25, 39]. We summarize our major contributions:

1. **MMEarth-Bench dataset:** We introduce five multimodal environmental monitoring tasks for benchmarking pretrained models. Each task consists of 12 aligned modalities and provides globally distributed data with both random and geographic test splits.
2. **Benchmarking:** We benchmark 7 recent pretrained models covering a range of architectures and including uni- and multimodal models. We find that all models still struggle to generalize geographically and that multimodal inputs can sometimes increase this gap.
3. **Method:** To advance model adaptation when labels are limited and geographically biased, we propose a test-time training method that uses modality reconstruction losses as a test-time adaptation signal. Our model-agnostic approach yields performance improvements across all models and tasks and both test splits.

## 2. Related work

### 2.1. Low-shot learning

**Pretrained geospatial models.** One strategy to facilitate low-shot learning is self-supervised pretraining. In contrast to vision foundation models trained on web data [15, 56], pretrained EO models are trained on large amounts of unlabeled remotely sensed data. While some geospatial models are still pretrained on RGB imagery [4, 32, 36, 51, 56], more recent unimodal models include additional spectral bands [6, 14, 42]. We benchmark a diverse set of pretrained models for global adaptation with limited and geographically biased labels, as found in real EO applications.

**Multimodal fusion.** Subsequently, additional work aimed to learn richer geospatial representations by pretraining on multimodal data [3, 28, 63, 67] or training multimodal models from scratch [50]. We evaluate the benefits of modality fusion in *pretrained* models under geographic shifts. Moreover, whereas multimodal models use multiple modalities as input, our TTT method uses them as *targets*.

**Joint training (JT).** Joint training trains a model simultaneously on both a main task and a self-supervised task in order to improve robustness on the main task, especially when training data is limited [26, 57, 59]. The model has a shared encoder and separate heads for the main task and auxiliary self-supervised tasks [57]. This method only uses multimodal data to generate reconstruction losses at train time. In contrast, our method also leverages the reconstruction losses as an *adaptation signal at test time*. We use JT as a baseline in our test-time training experiments.

### 2.2. Domain adaptation

**Unsupervised domain adaptation (UDA).** Unsupervised domain adaptation uses labeled data from the source domain and unlabeled data from the target domain to adapt to the target domain [34]. The UDA-SS [58] method extends JT by including unlabeled target data during the training process to facilitate the encoder’s adaptation to the target domain. Like many common UDA methods, this is primarily designed for covariate shifts across domains [33, 34]. The geographic generalization problem differs, as we also encounter *label* distribution shifts. Scheibenreif et al. [53] inserts adapters into a pretrained encoder and trains them with SSL using target domain modalities before finetuning the model with target domain labels. In contrast, our problem setup assumes that we neither have access to labeled nor unlabeled data from the target domain during training. Our model-agnostic approach also avoids modifying the encoder architecture.

**Test-time adaptation (TTA).** Unlike traditional UDA which uses target distribution data during training, test-time adaptation updates the model during testing to address distribution shifts [23, 59]. Following JT, rather than discard-

ing the self-supervised task head [58], TTT uses this head at test time to calculate a loss for adapting the encoder before making a final prediction [23, 59]. To avoid having to define a self-supervised auxiliary task, TENT [62] uses the prediction entropy as an adaptation signal. This makes it a natural approach for classification tasks but not for regression, which is common for biophysical variables (4 of our 5 tasks). Unlike TENT, which updates the encoder’s batch norm statistics, our proposed TTT method works with any architecture and loss. This is especially relevant as many pretrained EO models use a transformer architecture without batch norm layers. While TTA has been used with remote sensing imagery to adapt to distribution shifts in street-level RGB imagery [64] and guide robots’ search for targets in an environment [39], we adapt pretrained models to *diverse* environmental tasks and domains at *global* scales.

**Regularization in TTA.** Regularization is crucial for TTA [25, 39], and simply using batched test data is a regularization method, as it results in less noisy gradients [43, 74]. Test batches can be comprised of multiple augmentations of a single image [59] or just be random samples of the test data [23]. We propose geographic batching as a compromise between regularization and specialization. Updating only the batch norm parameters [62] or FiLM layers [44, 71] are commonly used regularization approaches. In model-agnostic fashion, our method uses batched test data along with 12 modality reconstruction losses, as opposed to a single adaptation signal, for regularization. Each individual modality’s gradient may be noisy, but averaging over them reduces noise. In this way, we avoid needing to insert batch norm or FiLM layers. The S4T method [29] uses a vision transformer as a task behavior synchronizer to lessen degradations in model performance due to the ideal number of TTT iterations differing among multiple auxiliary tasks. We achieve regularization with a lightweight linear task modality decoder.

**Multimodal TTA.** Shin et al. [54] studies multimodal TTA for 3D semantic segmentation by producing pseudo-labels for use as a self-training signal at test time given RGB images and LiDAR point clouds. Like TENT, their method updates batch norm parameters in the architecture. READ [68] addresses the scenario where modalities vary in their reliability when subject to domain shifts. They encode each modality with a transformer and modulate attention-based fusion layers at test time. Unlike READ, our approach does not require encoding the auxiliary modalities, instead solely using them as reconstruction targets.

### 2.3. Existing benchmark datasets

**Overview.** Past work in benchmark datasets for pretrained EO models has guided progress in model development and pretraining strategies. We summarize the most related benchmarks in Tab. 1. *SustainBench* [70] is a collection of

Table 1. **Comparison of benchmark datasets for EO (vision) foundation models.** “M” is the number of modalities per task. “✓/✗” means a property holds for a subset of tasks.

Benchmark	Domain	M	Global	Climate
Copernicus-Bench [63]	Mixed	1	✓/✗	✓/✗
PANGAEA [37]	Mixed	1-3	✓/✗	✗
PhilEO Bench [22]	Built-up	1	✓	✗
FoMo-Bench [10]	Forests	1-4	✓/✗	✓/✗
GEO-Bench [30]	Mixed	1-3	✗	✗
SustainBench [70]	SDGs	1-10	✓/✗	✗
MMEarth-Bench (ours)	Nature	12	✓	✓

15 tasks designed to track progress in 7 sustainable development goals, including no poverty, quality education, and climate action. The modalities vary by task and can include imagery from Landsat, Sentinel-2 (S2), MODIS, NAIP, as well as geolocation and time. *GEO-Bench* [30] contains 12 tasks ranging from building and solar panel classification to tree segmentation. The modalities vary by task and can include S2, Sentinel-1 (S1), Landsat-8, RGB, hyperspectral imagery, or elevation data. None of the tasks are globally distributed. *FoMo-Bench* [10] contains 15 datasets for forest monitoring, where each task has up to 4 modalities such as S2, S1, LiDAR, elevation, or meteorological data. *PhilEO Bench* [22] contains task data for building density estimation, road segmentation, and landcover classification. All tasks have S2 as the single input modality. *Copernicus-Bench* [63] is a benchmark focusing on cross-modal model evaluation that includes 15 unimodal tasks including land cover, biomass, and air quality. The input modality varies across tasks and can include sensors such as Sentinel-1, -2, -3, or -5P. *PANGAEA* [37] is a collection of existing benchmark datasets, each of which has up to 3 modalities such as S2, S1, Planet [47], or Maxar [38].

**Limitations.** None of the existing benchmark datasets share the same multiple modalities across all downstream tasks, and the vast majority of tasks contain no more than 3 modalities. This limits the evaluation of multimodal pretrained models, since likely not all of their modalities are available at test time. Furthermore, the vast majority of downstream tasks are limited to a single geographic region. Even if a benchmark contains tasks covering different regions, this does not make it possible to determine whether a pretrained model is able to generalize from one region to another. While PANGAEA explicitly mentions a geographic test split for one task and SustainBench includes geographic splits for several tasks, benchmarks rarely explicitly state whether a test split represents an entire held-out region or simply avoids overlap with the training data. This is likely due to a combination of geographic generalization not being prioritized and many benchmarks collect-

Table 2. MMEARTH-BENCH tasks.

Task	# Tiles	Unit	Scale	Type	License
Biomass	18,393	Mg/ha	Pixel-level	Regression	CC BY
Soil N	5,643	g/kg	Tile-level	Regression	CC BY-NC
Soil OC	7,982	g/kg	Tile-level	Regression	CC BY-NC
Soil pH	8,508	Unitless	Tile-level	Regression	CC BY-NC
Species	36,410	Presence/absence	Tile-level	Multi-label classification	Terms of Use

ing existing datasets and using their data splits. The degree to which a geographic test split can be a distribution shift is also limited by the geographic spread of the data in the first place. Additionally, few downstream tasks include climate data as a modality, limiting development in fusion methods for optical EO and climate data. While there are several downstream tasks focusing on the natural world, many tasks focus on the human-nature interface and the built-up world. Moreover, the same tasks appear in multiple benchmarks, most of which include preexisting datasets. We contribute five novel, global datasets for evaluating pretrained models on biomass, soil property, and species occurrence prediction. Our tasks focus on the natural world with 12 shared modalities across imagery, map products, and climate variables. These design choices should facilitate future development of multimodal models.

### 3. MMEARTH-BENCH Dataset

**Dataset overview.** MMEARTH-BENCH is comprised of five new datasets, summarized in Tab. 2, for environmental downstream tasks: aboveground biomass, soil nitrogen (N), soil organic carbon (OC), soil pH, and species occurrence. Each single-timestamp dataset includes 12 modalities along with task data for each  $128 \times 128$ -pixel tile. Every pixel represents 10m on the ground, so each tile spans an area of  $\approx 1.6 \text{ km}^2$ . All five tasks share the same 12 modalities (see Tab. 3) present in the MMEarth pretraining dataset [42]. Within each task, we ensure no overlap among tiles. Note that the datasets in MMEARTH-BENCH are not designed for producing the next best task-specific model or for time-series modeling. Rather, we design our datasets to be informative tools for the evaluation of pretrained models that hope to generalize to a variety of downstream tasks with limited data under geographic shifts.

**Data splits.** The tiles from each task are split into train, validation, random test, and geographic test sets (see Fig. 2). The tiles in Africa define the geographic test set, as it is often underrepresented in labeled data derived from field measurements, as is the case for our soil tasks [27, 65]. The remaining tiles are randomly split into train/validation/random test with ratios 70%/15%/15%. We include both a random and a geographic test set to evaluate model performance both in- and out-of-distribution. In practice one

Table 3. MMEARTH-BENCH modalities.

Modality	Bands	Scale	Type
Sentinel-2 (S2)	B1, B2, B3, B4, B5, B6, B7, B8, B8A, B9, B11, B12	Pixel	Continuous
Sentinel-1 (S1)	Ascending VV, VH, HH, HV; Descending VV, VH, HH, HV	Pixel	Continuous
ASTER GDEM	Elevation, slope	Pixel	Continuous
ETH Global Canopy Height	Height, uncertainty	Pixel	Continuous
Dynamic World	Landcover	Pixel	Categorical
ESA WorldCover	Landcover	Pixel	Categorical
Precipitation	Previous month, month, year	Tile	Continuous
Temperature	Previous month max, mean, min; month max mean, min; year max, mean, min	Tile	Continuous
Geolocation	Longitude, latitude	Tile	Continuous
Sentinel-2 date	Date	Tile	Continuous
Biome	Biome number	Tile	Categorical
Ecoregion	Ecoregion number	Tile	Categorical

might expect models finetuned with non-Africa data to be used to make predictions in Africa, making it especially relevant to understand how effective this generalization actually is. To allow for evaluating models in very low data regimes, we also provide train sets containing 50% and 5% of the original training tiles, selected randomly but where the 5% train set is a subset of the 50% train set.

**Modalities.** All of our tiles include 12 modalities, six of which are pixel-level (S2, S1, ASTER GDEM [41], ETH Global Canopy Height [31], Dynamic World [12] and ESA WorldCover [73]) and six of which are tile-level (ERA5 precipitation and temperature, geolocation, Sentinel-2 date, biome and ecoregion [16]). The modalities also represent a combination of continuous- and categorical-valued data. All of the modality data is accessed through Google Earth Engine (GEE) [24]. If users wish to augment their set of modalities for TTT on a new task, they can use our code to extract the MMEarth modalities simply by providing the (lon, lat) coordinates for their task data.

**Tasks.** Our biomass dataset is sourced from aboveground biomass estimates from NASA’s 2020 GEDI mission [17]. We sample measurements with GEE such that our tiles are approximately balanced across biomes. We obtain our soil data from the WoSIS December 2023 snapshot [7]. We select soil N, soil OC, and soil pH due to their environmental and ecological significance. Nitrogen is crucial for plant growth, organic carbon is an indicator of soil quality, and pH has a strong influence on biogeochemical processes in soil [69]. For each soil property we aggregate data across time within the depth range 0-5 cm. Biomass and the soil properties are regression tasks. We extract our species range data from the IUCN Red List’s terrestrial mammal range polygons [1]. We filter by species whose historic range covers at least 6,000  $\text{km}^2$  both in and outside Africa and then take the first 100 species. Sampling tiles from these overlapping ranges yields multiple species per tile, making

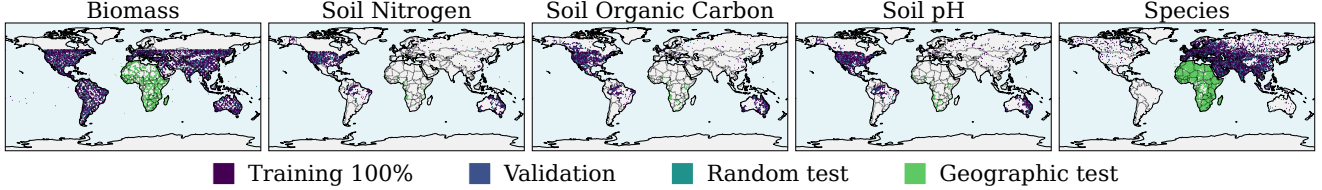


Figure 2. **Data splits in MMEARTH-BENCH.** Each of the 5 tasks consists of a geographic test split (“Africa”) and splits the rest of the world randomly into training (70%), validation (15%), and random test (15%). While the full training dataset is shown here, we also provide subsets with 50% and 5% of the training data for even lower-shot experiments.

this a multi-label classification task. The minimum number of tiles in which a species appears by split is 187 for train 100%, 101 for train 50%, 7 for train 5%, 32 for validation, 46 for random test, and 173 for geographic test. See the Supplementary for more details.

## 4. Methodology

**Multimodal adaptation signal.** We propose a method for multimodal test-time training, TTT-MMR, in which we formulate reconstruction tasks using the *task modalities*, *i.e.* the set of modalities available at test time. A task modality decoder is used to reconstruct all the task modalities given the encoder’s embedding of the *input modalities*, *i.e.* the subset of modalities accepted by the encoder. For a given task, we first perform joint training (JT, Sec. 2.1), during which we train the task modality decoder with the mean of the modality reconstruction losses, the main task decoder with the task loss, and the encoder with the sum of these two losses. Then at test time the reconstruction losses serve as adaptation signals for the encoder (see Fig. 3). TTT-MMR normalizes the gradients of the task modality reconstruction losses per modality and then averages them across modalities (excluding missing modalities) so that each modality contributes equally to the adaptation signal, regardless of its original scale. We keep the task modality decoder frozen to force the encoder to adapt.

**Formalization.** Each batch  $B$  contains a set of  $|B|$  tiles.

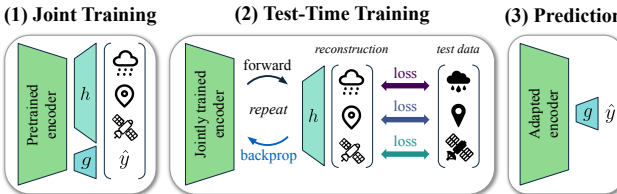


Figure 3. **TTT with multimodal reconstruction (TTT-MMR).** (1) We adapt a pretrained encoder to a downstream task by jointly training the encoder together with the main task decoder  $g$  and task modality decoder  $h$ . At test time, for each batch: (2) the modality reconstruction losses are used to adapt the encoder iteratively, and (3) the adapted encoder is used to yield improved predictions.

Each tile  $t \in B$  has data for the input modalities, collectively  $i_t$ , and data for each task modality  $m \in M$  given by  $d_{m,t}$ . Let the encoder be a function  $e_\theta$  of the input modalities with parameters  $\theta$ . Then  $\{e_\theta(i_t)\}_{t \in B}$  are the input embeddings. Let the task modality decoder be a function  $h$  with parameters  $\alpha$  of the input embeddings. It produces a reconstruction  $h_\alpha(e_\theta(i_t))_{m,t}$  for each task modality  $m$  for every tile  $t$  in the batch. Let  $R_{m,t}(d_{m,t}, h_\alpha(e_\theta(i_t))_{m,t})$  be the reconstruction loss between tile  $t$ ’s modality  $m$  and its reconstruction by  $h_\alpha$ . For each modality, the reconstruction loss is averaged across all tiles in the batch:

$$R_m = \frac{1}{|B|} \sum_{t \in B} R_{m,t}(d_{m,t}, h_\alpha(e_\theta(i_t))_{m,t}). \quad (1)$$

We take the gradient of each per-modality reconstruction loss with respect to the encoder parameters:  $\frac{\partial R_m}{\partial \theta} = \frac{\partial R_m}{\partial h_\alpha} \frac{\partial h_\alpha}{\partial e_\theta} \frac{\partial e_\theta}{\partial \theta}$ . To put equal weight on each modality, we separately normalize their gradients,  $\frac{\partial R_m}{\partial \theta} \rightarrow \frac{1}{\|\frac{\partial R_m}{\partial \theta}\|} \frac{\partial R_m}{\partial \theta}$ , before averaging the gradients across modalities. We finally adapt the parameter  $\theta_j$  by backpropagating this mean gradient using stochastic gradient descent with learning rate  $\lambda$ :

$$\theta_j \rightarrow \theta_j - \frac{\lambda}{|M|} \sum_{m \in M} \frac{1}{\|\frac{\partial R_m}{\partial \theta}\|} \frac{\partial R_m}{\partial \theta_j}. \quad (2)$$

In an iterative optimization process, we can use the updated encoder to generate new embeddings and reconstructions to compute new reconstruction losses and gradients, which can then update the encoder again. After TTT, the adapted encoder  $e_{\theta'}$  produces embeddings that the task decoder  $g$  uses to generate a final prediction, after which the encoder is reset to its post-JT state for the next batch. We determine the number of TTT iterations by performing  $I_{\max}$  iterations on every batch in the validation set and then use the mean of the batches’ best iteration number during testing. In our experiments, we use  $|B| = 8$ ,  $\lambda = 10^{-2}$ , and  $I_{\max} = 5$ .

**Batching.** We compare TTT-MMR, in which batches are random, non-overlapping samples of the test data, with TTT-MMR-GEO, which batches the test data based on geographic proximity as a proxy for sample similarity. The latter allows specialization to the geographic domain defined by the batch, at the cost of some regularization that comes from averaging over more geographically diverse

Table 4. Pretrained models benchmarked.

Method	Architecture	Pretraining dataset	Input modalities
Scale-MAE [51]	ViT-L	FMoW-RGB [13]	RGB
DINOv3 Web [56]	ViT-L/16 distilled	LVD-1689M [56]	RGB
DINOv3 Sat [56]	ViT-L/16 distilled	SAT-493M [56]	RGB
SatlasNet [6]	Swin-v2-B	SatlasPretrain [6]	S2
MPMAE [42]	ConvNeXt V2-A	MMEarth [42]	S2
TerraMind [28]	TerraMindv1-B	TerraMesh [9]	S2, S1, DEM, RGB
Copernicus-FM [63]	ViT-B	Copernicus-Pretrain [63]	S2, S1, DEM, Geolocation, Date

tiles. We generate the geographic batches through recursive spatial partitioning, mimicking a k-d tree [8]. We recursively subdivide the region containing the split’s tiles into smaller and smaller rectangles until only one sub-region has more than  $|B|$  tiles. This results in non-overlapping batches that are contiguous geographic regions.

## 5. Experimental results

In this section, we address the following research questions:

1. *How well can pretrained models transfer to downstream tasks with limited reference data?*
2. *Can pretrained models generalize geographically?*
3. *When do pretrained multimodal models benefit from using multiple input modalities at test time?*

Lastly, we demonstrate that multimodal TTT improves pretrained models with limited and geographically biased data.

### 5.1. Setup

**Benchmarking.** We benchmark 7 pretrained models: 3 RGB-only, 2 S2-only, and 2 multimodal models (see Tab. 4). For comparison, we also evaluate a randomly initialized ConvNeXtV2A model with RGB input. All methods use a linear task decoder. For the tile-level tasks, the task decoder consists of global average pooling followed by layer norm and a fully connected layer, and for the pixel-level task, it bilinearly upsamples the embeddings to the tile size and then applies a convolutional layer with a  $1 \times 1$  kernel. We finetune by training all model parameters. Linear probing results are provided in the Supplementary.

**Multimodal models.** The TerraMind encoder consists of a series of blocks in which modality-specific tokens are conditioned on one another through the attention mechanism. For modality fusion, we use the default implementation, which averages the patch embeddings from the final encoder block across modalities. In contrast, cross-modal Copernicus-FM does not have per-modality encoding. We implement it as a Siamese network, sharing parameters across modalities. We separately compute embeddings for S2, S1, and DEM and then average them.

**JT and TTT.** JT and TTT use a linear task modality decoder that first bilinearly upsamples the input embeddings to the tile size. It then passes them through a 2D convolution with a  $1 \times 1$  kernel that reconstructs every band in ev-

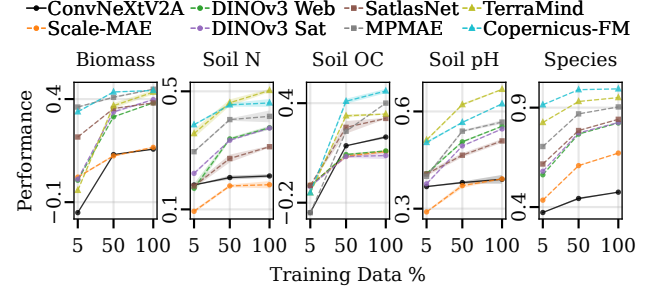


Figure 4. **Low-shot in-distribution performance.** Finetuning on subsets of the training data. Symbology: •=RGB, ■=S2, ▲=multimodal, solid=random init., dashed=pretrained.

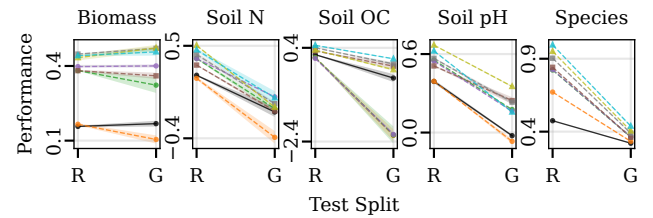


Figure 5. **Geographic generalization.** Performance comparison on random (R) vs. geographic (G) test splits using all training data.

ery task modality at the tile resolution. We group the channels by modality and perform global average pooling on the bands of the tile-level modalities, yielding our modality reconstructions. In computing the reconstruction losses we use cross-entropy loss for the categorical-valued modalities and MSE loss for the continuous-valued modalities.

**Implementation.** We run our experiments on an NVIDIA H200 140GB GPU. We train for 100 epochs with batch size 64. We use a maximum learning rate of  $10^{-4}$  and a weight decay of 0.05 [37]. We use the AdamW optimizer [35] and a learning rate scheduler with a linear warm-up of 10 epochs followed by cosine annealing [63] with a minimum learning rate of  $10^{-6}$  [5]. The regression tasks use MSE loss and species uses BCE with logits loss. In all results, “performance” refers to  $R^2$  for the regression tasks and mean average precision (mAP) for species. Following training, we select the checkpoint with the highest performance on the validation set and run it on the two test sets to obtain our results. We normalize the data fed into the pretrained models using their indicated normalization method and statistics. For the randomly initialized model and the task modalities, we center-normalize using the mean and STD of the bands in the training dataset. All experiments reflect the results of three distinct random seeds. Shaded regions in plots reflect 1 standard error across seeds.

## 5.2. Transfer learning with limited reference data

We finetune all 7 pretrained models and the randomly initialized ConvNeXtV2A on three subsets of the training data: 5%, 50%, and 100%. We then evaluate the models on the random, in-distribution test split to determine how effectively they transfer to the five tasks in MMEARTH-BENCH, with results shown in Fig. 4. Overall, we see that the pretrained models tend to outperform the randomly initialized model across tasks and training subsets.

For tasks other than species, the randomly initialized model performs similarly to or better than at least one of the models pretrained only on RGB. Overall, the two multimodal models perform best, with MPMAE, an S2-only model, showing competitive or superior performance to the multimodal models on the biomass and soil OC tasks especially. The species task displays the largest spread in model performance and also clearest and most consistent model rankings across training data subsets. The RGB-only models underperform relative to the multispectral models overall. Biomass and soil OC appear to be most sensitive to limited training data, with none of the models achieving a positive  $R^2$  with only 5% of the training data on the soil OC task, which existing work in soil modeling has found to be a challenging task [21]. Comparing DINOv3 Web and DINOv3 Sat, we see that the domain-specific pretraining of DINOv3 Sat had little benefit on our tasks. Together, our results show that multimodal pretraining with multimodal evaluation leads to better performance on our environmental tasks, but there is still substantial room for improvement when task training data is limited.

Originally, Copernicus-FM [63] used multimodal inputs in a linear probing setting, where it does not matter whether one learns separate modality-specific encoders or shares parameters across modalities (as we do). This is, however, relevant for finetuning, where a cross-modal evaluation with unimodal tasks was originally performed. We provide a *multimodal* finetuning evaluation of Copernicus-FM.

## 5.3. Geographic generalization challenge

Next, we evaluate all the models on the geographic test split after finetuning on all the training data to determine how effectively they generalize to Africa, for which they have not seen labels. As shown in Fig. 5, for all tasks except biomass, the models experience substantial performance drops when switching from the random to the geographic test split.

This large deterioration in performance reveals that globally pretrained models still struggle with out-of-distribution data. For soil N and soil OC, even the multimodal models struggle on the geographic split. The randomly initialized model sometimes outperforms the pretrained RGB-only models on Africa, but it still underperforms relative to the multispectral models. These results suggest that soil N and soil OC are especially challenging to predict in new

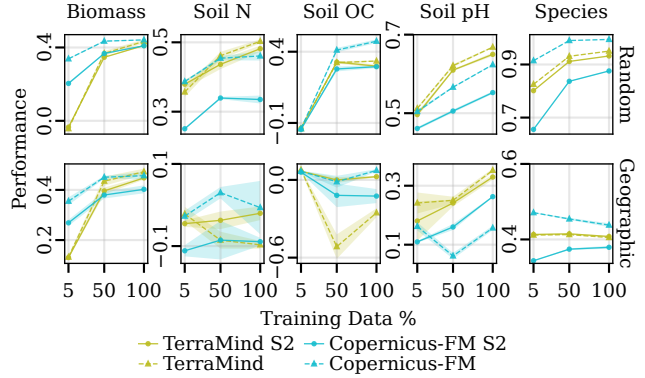


Figure 6. **Unimodal vs. multimodal input data.** Finetuning performance of S2-only (solid-circle) versus multimodal (dashed-triangle) variants of TerraMind and Copernicus-FM.

regions. All the soil tasks and species occurrence offer an opportunity for globally pretrained models to improve their methodology to better facilitate geographic generalization on downstream tasks. The DINOv3 models have likely seen unlabeled data from Africa during pretraining, and the other pretrained models have for sure. All models have seen labeled task data from the rest of the world during finetuning. Our results suggest that the representations learned for Africa during pretraining are either uninformative for some of our tasks or that finetuning on the world without Africa erases some of the information encoded about the region, hindering geographic generalization.

## 5.4. The effect of multimodal input data

We compare multimodal and S2-only variants of TerraMind and Copernicus-FM to evaluate the effect of multimodal input data on their performance. Fig. 6 shows that the models can use the additional modalities to produce better task-specific representations on both the random and geographic test splits. While the multimodal version usually outperforms the unimodal one, there are a couple of exceptions in the geographic split of the soil tasks. While Fig. 5 showed that multimodal pretraining tends to lead to better geographic generalization than unimodal pretraining, Fig. 6 suggests that *finetuning* the same model with multi- rather than unimodal inputs can harm generalization. The additional modalities could lead to overfitting to the non-Africa training domain, which is harmful if the modalities undergo domain shifts between non-Africa and Africa. This effect appears more strongly for TerraMind than Copernicus-FM, which could be because our Siamese Copernicus-FM simply averages embeddings across modalities, but the fusion is learned in TerraMind. This result is consistent with prior work which found that finetuning modality fusion modules could lead to geographic overfitting [50]. Furthermore, TerraMind has modality-specific encoders and thus more ca-

Table 5. **Multimodal test-time training improvement per model.** Average ranks of JT (joint training baseline), TTT-MMR (random batching), and TTT-MMR-GEO (geographic batching). Ranks are mean  $\pm$  standard error averaged over tasks and seeds. Lower is better.

Split	Method	ConvNeXtV2A	Scale-MAE	DINOv3 Web	DINOv3 Sat	SatlasNet	MPMAE	TerraMind	Copernicus-FM
Random	JT	2.9 $\pm$ 0.1	3.0 $\pm$ 0.0	3.0 $\pm$ 0.0	3.0 $\pm$ 0.0	2.9 $\pm$ 0.1	3.0 $\pm$ 0.0	3.0 $\pm$ 0.0	2.8 $\pm$ 0.1
	TTT-MMR	2.1 $\pm$ 0.1	1.8 $\pm$ 0.1	1.8 $\pm$ 0.1	1.7 $\pm$ 0.1	1.8 $\pm$ 0.1	1.6 $\pm$ 0.1	<b>1.5 <math>\pm</math> 0.1</b>	1.7 $\pm$ 0.2
	TTT-MMR-Geo	<b>1.1 <math>\pm</math> 0.1</b>	<b>1.2 <math>\pm</math> 0.1</b>	<b>1.2 <math>\pm</math> 0.1</b>	<b>1.3 <math>\pm</math> 0.1</b>	<b>1.3 <math>\pm</math> 0.1</b>	<b>1.4 <math>\pm</math> 0.1</b>	<b>1.5 <math>\pm</math> 0.1</b>	<b>1.5 <math>\pm</math> 0.1</b>
Geographic	JT	3.0 $\pm$ 0.0	2.8 $\pm$ 0.1	3.0 $\pm$ 0.0	3.0 $\pm$ 0.0	2.7 $\pm$ 0.2	2.7 $\pm$ 0.2	2.9 $\pm$ 0.1	2.8 $\pm$ 0.1
	TTT-MMR	<b>1.5 <math>\pm</math> 0.1</b>	1.9 $\pm$ 0.2	1.7 $\pm$ 0.1	<b>1.5 <math>\pm</math> 0.1</b>	<b>1.6 <math>\pm</math> 0.2</b>	2.0 $\pm$ 0.1	1.7 $\pm$ 0.1	1.8 $\pm$ 0.1
	TTT-MMR-Geo	<b>1.5 <math>\pm</math> 0.1</b>	<b>1.3 <math>\pm</math> 0.1</b>	<b>1.3 <math>\pm</math> 0.1</b>	<b>1.5 <math>\pm</math> 0.1</b>	1.7 $\pm$ 0.2	<b>1.3 <math>\pm</math> 0.2</b>	<b>1.3 <math>\pm</math> 0.2</b>	<b>1.4 <math>\pm</math> 0.2</b>

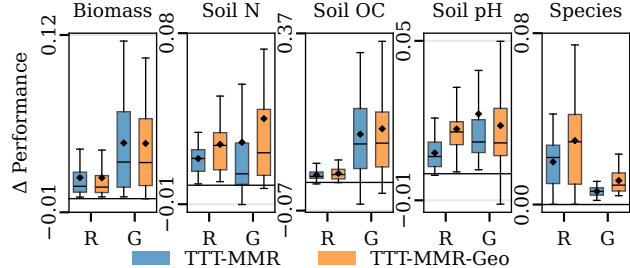


Figure 7. **Multimodal test-time training improvement per task.** Improvement of TTT-MMR (random batching) and TTT-MMR-GEO (geographic batching) over joint training. Boxplots show the distribution over all models and seeds.  $\blacklozenge$ =mean,  $=$ median, whiskers are based on the 1.5 IQR value.  $\Delta$  Performance reflects the absolute change in the performance metric.

pacity to fit the training data.

### 5.5. Multimodal test-time training performance

After performing JT, we apply TTT-MMR or TTT-MMR-GEO to the models to improve performance. Fig. 7 shows that both of our proposed approaches improve performance over JT on all tasks. For biomass and soil OC both variants perform similarly, with TTT-MMR-GEO displaying better performance on soil N, soil pH, and species. One-sided (greater) Wilcoxon tests with Holm-Bonferroni correction demonstrate statistical significance of the performance improvement after TTT for each boxplot with  $p < 0.01$ . In addition, both methods improve performance on the random *and* the geographic test split, with larger gains on the geographic split for biomass and soil OC. Thus, our proposed TTT methods boost model performance with a maximum of five update iterations to the encoder.

Looking at method rankings per model averaged over tasks in Tab. 5, we see that both our TTT methods outperform JT for all models. TTT-MMR-GEO is the best method for all models except SatlasNet, indicating that it may benefit from the additional regularization that comes from random batching. We find that the RGB-only models tend to undergo larger performance improvements as a result of TTT than the multispectral and multimodal models (see additional results in the Supplementary). These are the

models that otherwise have the least ‘information’ about a given tile, but both TTT-MMR variants allow them to make use of multimodal data. The S2 and multimodal models still get additional modalities through TTT-MMR but also get more spectral information as input. Although MPMAE was pretrained by reconstructing these same modalities, we do not observe any special behavior in its performance gains from TTT. Overall, all benchmarked models benefit from our methods, despite having diverse architectures, pretraining strategies, and input modalities. This demonstrates that our TTT methods are model-agnostic and task-agnostic.

Combining all 12 task modality reconstruction losses helps prevent overfitting to any single reconstruction task, producing a more robust adaptation signal that is more likely to align with the actual task of interest. We also find that our per-modality gradient normalization improves stability during TTT.

## 6. Conclusion

Models pretrained on large, unlabeled Earth observation datasets aim to generalize to new tasks and geographic domains with limited data as well as resolve ambiguities by fusing multiple modalities. To evaluate progress towards these goals, we present MMEARTH-BENCH, a new multimodal benchmark dataset that contains 12 aligned EO modalities and task data for biomass, soil nitrogen, soil organic carbon, soil pH, and species occurrence. We benchmark 7 pretrained models on these tasks and find that the multispectral ones perform better than the RGB-only models, but all models exhibit a geographic generalization gap on 4 out of 5 tasks. We also demonstrate that using multiple input modalities at test time helps in-distribution but can sometimes lead to overfitting under geographic shifts. Towards overcoming these challenges, we introduce test-time training with multimodal reconstruction (TTT-MMR), which uses multiple modalities as reconstruction tasks at test time to provide a self-supervised adaptation signal for the encoder. Our results show that TTT-MMR can lead to improved performance on all models, tasks, and splits over a joint training baseline. Thus, we have formulated an efficient, model-agnostic method for improving adaptation performance at test time.

**Acknowledgments** We greatly appreciate the open data policies of the Copernicus program and its partners ESA and ECMWF. We thank Google Earth Engine for hosting the data and providing free access. We also appreciate access to Harvard’s FAS Research Computing cluster. This work was supported in part by the Pioneer Centre for AI, DNRF grant number P1, by the research grant Global Wetland Center (grant number NNF23OC0081089) from Novo Nordisk Foundation, and by the European Union project ELIAS (grant agreement number 101120237). LG was supported in part by the National Science Foundation Graduate Research Fellowship under Grant No. DGE 2140743.

## References

- [1] IUCN 2025. The IUCN Red List of Threatened Species. *Version 2025-1*, Downloaded on June 13, 2025. [4](#), [15](#)
- [2] Dominique Arrouays, Michael G. Grundy, Alfred E. Hartemink, Jonathan W. Hempel, Gerard B.M. Heuvelink, S. Young Hong, Philippe Lagacherie, Glenn Lelyk, Alexander B. McBratney, Neil J. McKenzie, Maria d.L. Mendonca-Santos, Budiman Minasny, Luca Montanarella, Inakwu O.A. Odeh, Pedro A. Sanchez, James A. Thompson, and Gan-Lin Zhang. Chapter three - globalsoilmap: Toward a fine-resolution global grid of soil properties. Academic Press, 2014. [15](#)
- [3] Guillaume Astruc, Nicolas Gonthier, Clément Mallet, and Loïc Landrieu. AnySat: One Earth Observation Model for Many Resolutions, Scales, and Modalities. In *CVPR*, 2025. [1](#), [2](#)
- [4] Kumar Ayush, Burak Uzkent, Chenlin Meng, Kumar Tanmay, Marshall Burke, David Lobell, and Stefano Ermon. Geography-aware self-supervised learning. *ICCV*, 2021. [2](#)
- [5] Roman Bachmann, David Mizrahi, Andrei Atanov, and Amir Zamir. MultiMAE: Multi-modal Multi-task Masked Autoencoders. *ECCV*, 2022. [6](#)
- [6] Favyen Bastani, Piper Wolters, Ritwik Gupta, Joe Ferdinando, and Aniruddha Kembhavi. SatlasPretrain: A Large-Scale Dataset for Remote Sensing Image Understanding. In *ICCV*, Los Alamitos, CA, USA, 2023. IEEE Computer Society. [2](#), [6](#), [20](#)
- [7] Niels H. Batjes, Luis Calisto, and Luis M. de Sousa. Providing quality-assessed and standardised soil data to support global mapping and modelling (WoSIS snapshot 2023). *Earth System Science Data*, 2024. [4](#), [14](#)
- [8] Jon Louis Bentley. Multidimensional binary search trees used for associative searching. *Commun. ACM*, 1975. [6](#)
- [9] Benedikt Blumenstiel, Paolo Fraccaro, Valerio Marsocci, Johannes Jakubik, Stefano Maurogiovanni, Mikolaj Czerkawski, Rocco Sedona, Gabriele Cavallaro, Thomas Brunschwiler, Juan Bernabe-Moreno, and Nicolas Longépé. TerraMesh: A Planetary Mosaic of Multimodal Earth Observation Data, 2025. [6](#), [20](#)
- [10] Nikolaos Ioannis Bountos, Arthur Ouaknine, Ioannis Poutsis, and David Rolnick. FoMo: multi-modal, multi-scale and multi-task remote sensing foundation models for forest monitoring. In *AAAI*. AAAI Press, 2025. [2](#), [3](#)
- [11] C.F. Brown, S.P. Brumby, and B. Guzder-Williams et al. Dynamic World, Near real-time global 10 m land use land cover mapping. [doi:10.1038/s41597-022-01307-4](https://doi.org/10.1038/s41597-022-01307-4), 2022. [18](#)
- [12] Christopher F Brown, Steven P Brumby, Brookie Guzder-Williams, Tanya Birch, Samantha Brooks Hyde, Joseph Mazzariello, Wanda Czerwinski, Valerie J Pasquarella, Robert Haertel, Simon Ilyushchenko, et al. Dynamic world, near real-time global 10 m land use land cover mapping. *Scientific data*, 2022. [4](#)
- [13] Gordon Christie, Neil Fendley, James Wilson, and Ryan Mukherjee. Functional Map of the World. In *CVPR*, 2018. [6](#), [20](#)
- [14] Yezhen Cong, Samar Khanna, Chenlin Meng, Patrick Liu, Erik Rozi, Yutong He, Marshall Burke, David B. Lobell, and Stefano Ermon. SatMAE: Pre-training transformers for temporal and multi-spectral satellite imagery. In *NeurIPS*, 2022. [2](#)
- [15] Jia Deng, Wei Dong, Richard Socher, Li-Jia Li, Kai Li, and Li Fei-Fei. ImageNet: A large-scale hierarchical image database. In *CVPR*, 2009. [2](#)
- [16] E Dinerstein, D Olson, A Joshi, C Vynne, ND Burgess, E Wikramanayake, N Hahn, S Palminteri, P Hedao, R Noss, et al. An ecoregion-based approach to protecting half the terrestrial realm. *BioScience*, 2017. [4](#), [12](#)
- [17] Ralph Dubayah, James Bryan Blair, Scott Goetz, Lola Fatoyinbo, Matthew Hansen, Sean Healey, Michelle Hofton, George Hurt, James Kellner, Scott Luthcke, et al. The global ecosystem dynamics investigation: High-resolution laser ranging of the earth’s forests and topography. *Science of remote sensing*, 2020. [4](#)
- [18] R.O. Dubayah, J. Armston, J.R. Kellner, L. Duncanson, S.P. Healey, P.L. Patterson, S. Hancock, H. Tang, J. Bruening, M.A. Hofton, J.B. Blair, and S.B. Luthcke. GEDI L4A Footprint Level Aboveground Biomass Density, Version 2.1. *ORNL DAAC*, Oak Ridge, Tennessee, USA, 2022. [12](#)
- [19] Laura Duncanson, James R Kellner, John Armston, Ralph Dubayah, David M Minor, Steven Hancock, Sean P Healey, Paul L Patterson, Svetlana Saarela, Suzanne Marselis, et al. Aboveground biomass density models for NASA’s Global Ecosystem Dynamics Investigation (GEDI) lidar mission. *Remote Sensing of Environment*, 270, 2022. [14](#)
- [20] Esri. World continents. [15](#)
- [21] C.J. Feeney, B.J. Cosby, and D.A. Robinson et al. Multiple soil map comparison highlights challenges for predicting topsoil organic carbon concentration at national scale. *Sci Rep* 12, 1379, 2022. [7](#)
- [22] Casper Fibæk, Luke Camilleri, Andreas Luysts, Nikolaos Dionelis, and Bertrand Le Saux. PhilEO Bench: Evaluating Geo-Spatial Foundation Models. In *IGARSS 2024 - 2024 IEEE International Geoscience and Remote Sensing Symposium*, 2024. [2](#), [3](#)
- [23] Yossi Gandelsman, Yu Sun, Xinlei Chen, and Alexei A Efros. Test-Time Training with Masked Autoencoders. In *NeurIPS*, 2022. [2](#), [3](#)
- [24] Noel Gorelick, Matt Hancher, Mike Dixon, Simon Ilyushchenko, David Thau, and Rebecca Moore. Google

Earth Engine: Planetary-scale geospatial analysis for everyone. *Remote Sensing of Environment*, 2017. 4

[25] Sachin Goyal, Mingjie Sun, Aditi Raghunathan, and Zico Kolter. Test-time adaptation via conjugate pseudo-labels. *NeurIPS*, 2022. 2, 3

[26] Dan Hendrycks, Kimin Lee, and Mantas Mazeika. Using Pre-Training Can Improve Model Robustness and Uncertainty. In *ICML*, 2019. 2

[27] iNaturalist contributors. iNaturalist Research-grade Observations. Occurrence dataset <https://doi.org/10.15468/ab3s5x> accessed via GBIF.org on 2025-11-10, 2025. 4

[28] Johannes Jakubik, Felix Yang, Benedikt Blumenstiel, Erik Scheurer, Rocco Sedona, Stefano Maurogiovanni, Jente Bosmans, Nikolaos Dionelis, Valerio Marsocci, Niklas Kopp, et al. TerraMind: Large-Scale Generative Multi-modality for Earth Observation. *ICCV*, 2025. 1, 2, 6, 20

[29] Wooseong Jeong, Jegyeong Cho, Youngho Yoon, and Kuk-Jin Yoon. Synchronizing Task Behavior: Aligning Multiple Tasks during Test-Time Training. In *ICCV*, 2025. 3

[30] Alexandre Lacoste, Nils Lehmann, Pau Rodriguez, Evan David Sherwin, Hannah Kerner, Björn Lütjens, Jeremy Andrew Irvin, David Dao, Hamed Alemohammad, Alexandre Drouin, Mehmet Gunturkun, Gabriel Huang, David Vazquez, Dava Newman, Yoshua Bengio, Stefano Ermon, and Xiao Xiang Zhu. GEO-Bench: Toward Foundation Models for Earth Monitoring. *NIPS*, 2023. 2, 3

[31] Nico Lang, Walter Jetz, Konrad Schindler, and Jan Dirk Wegner. A high-resolution canopy height model of the Earth. *Nature Ecology & Evolution*, 2023. 4, 18

[32] Wenyuan Li, Keyan Chen, Hao Chen, and Zhenwei Shi. Geographical knowledge-driven representation learning for remote sensing images. *IEEE Transactions on Geoscience and Remote Sensing*, 2021. 2

[33] Xiaofeng Liu, Zhenhua Guo, Site Li, Fangxu Xing, Jane You, C.-C. Jay Kuo, Georges El Fakhri, and Jonghye Woo. Adversarial unsupervised domain adaptation with conditional and label shift: Infer, align and iterate. In *ICCV*, 2021. 2

[34] Xiaofeng Liu, Chaehwa Yoo, Fangxu Xing, Hyejin Oh, Georges Fakhri, Je-Won Kang, and Jonghye Woo. Deep unsupervised domain adaptation: A review of recent advances and perspectives. *APSIPA Transactions on Signal and Information Processing*, 2022. 2

[35] Ilya Loshchilov and Frank Hutter. Decoupled weight decay regularization. In *ICLR*, 2017. 6

[36] Oscar Manas, Alexandre Lacoste, Xavier Giró-i Nieto, David Vazquez, and Pau Rodriguez. Seasonal contrast: Unsupervised pre-training from uncurated remote sensing data. In *ICCV*, 2021. 2

[37] Valerio Marsocci, Yuru Jia, Georges Le Bellier, David Kerekes, Liang Zeng, Sebastian Hafner, Sebastian Gerard, Eric Brune, Ritu Yadav, Ali Shibli, et al. Pangaea: A global and inclusive benchmark for geospatial foundation models. *arXiv preprint arXiv:2412.04204*, 2024. 1, 2, 3, 6

[38] Maxar Technologies. [maxar.com](https://maxar.com). 3

[39] Derek Ming, Siang Tan, Shailesh, Boyang Liu, Alok Raj, Qi Xuan Ang, Weiheng Dai, Tanishq Duhan, Jimmy Chiun, Yuhong Cao, Florian Shkurti, and Guillaume Sartoretti. Search-tta: A multimodal test-time adaptation framework for visual search in the wild. In *Conference on Robot Learning*. PMLR, 2025. 2, 3

[40] David Mizrahi, Roman Bachmann, Oğuzhan Fatih Kar, Teresa Yeo, Mingfei Gao, Afshin Dehghan, and Amir Zamir. 4M: Massively Multimodal Masked Modeling. In *NeurIPS*, 2023. 2

[41] NASA/METI/AIST/Japan Space Systems and U.S./Japan ASTER Science Team. Digital Elevation Model V003. <https://doi.org/10.5067/ASTER/ASTGTM.003>, 2018. 4

[42] Vishal Nedungadi, Ankit Kariyaa, Stefan Oehmcke, Serge Belongie, Christian Igel, and Nico Lang. MMEarth: Exploring multi-modal pretext tasks for geospatial representation learning. In *ECCV*. Springer, 2024. 1, 2, 4, 6, 20, 21

[43] Shuaicheng Niu, Jiaxiang Wu, Yifan Zhang, Zhiqian Wen, Yaofu Chen, Peilin Zhao, and Mingkui Tan. Towards Stable Test-Time Adaptation in Dynamic Wild World. In *ICLR*, 2023. 3

[44] Ethan Perez, Florian Strub, Harm de Vries, Vincent Dumoulin, and Aaron C. Courville. Film: Visual reasoning with a general conditioning layer. In *AAAI*, 2018. 3

[45] Claudio Persello, Jan Dirk Wegner, Ronny Hänsch, Devis Tuia, Pedram Ghamisi, Mila Koeva, and Gustau Camps-Valls. Deep learning and earth observation to support the sustainable development goals: Current approaches, open challenges, and future opportunities. *IEEE Geoscience and Remote Sensing Magazine*, 2022. 1

[46] Lukas Picek, Christophe Botella, Maximilien Servajean, César Leblanc, Rémi Palard, Théo Larcher, Benjamin Deneu, Diego Marcos, Pierre Bonnet, and Alexis Joly. Geoplant: Spatial plant species prediction dataset. In *NIPS*. Curran Associates, Inc., 2024. 2

[47] Planet. [planet.com](https://planet.com). 3

[48] L. Poggio, L. M. de Sousa, N. H. Batjes, G. B. M. Heuvelink, B. Kempen, E. Ribeiro, and D. Rossiter. Soilgrids 2.0: producing soil information for the globe with quantified spatial uncertainty. *SOIL*, 2021. 14

[49] Earthquake Hazards Program. Google earthtm/kml files. 15

[50] Arjun Rao and Esther Rolf. Using Multiple Input Modalities can Improve Data-Efficiency and O.O.D. Generalization for ML with Satellite Imagery. In *TerraBytes - ICML 2025 workshop*, 2025. 1, 2, 7

[51] Colorado J Reed, Ritwik Gupta, Shufan Li, Sarah Brockman, Christopher Funk, Brian Clipp, Kurt Keutzer, Salvatore Candido, Matt Uyttendaele, and Trevor Darrell. Scale-MAE: A Scale-Aware Masked Autoencoder for Multiscale Geospatial Representation Learning. In *ICCV*, Los Alamitos, CA, USA, 2023. IEEE Computer Society. 2, 6, 20

[52] Srikumar Sastry, Subash Khanal, Aayush Dhakal, Adeel Ahmad, and Nathan Jacobs. Taxabind: A unified embedding space for ecological applications. In *2025 IEEE/CVF Winter Conference on Applications of Computer Vision (WACV)*, 2025. 2

[53] Linus Scheibenreif, Michael Mommert, and Damian Borth. Parameter efficient self-supervised geospatial domain adaptation. In *Proceedings of the IEEE/CVF Conference on Computer Vision and Pattern Recognition (CVPR)*, 2024. 2

[54] Inkyu Shin, Yi-Hsuan Tsai, Bingbing Zhuang, Samuel Schulter, Buyu Liu, Sparsh Garg, In So Kweon, and Kuk-Jin Yoon. MM-TTA: Multi-Modal Test-Time Adaptation for 3D Semantic Segmentation. In *CVPR*, 2022. 3

[55] Ghjulia Sialelli, Torben Peters, Jan D. Wegner, and Konrad Schindler. AGBD: A Global-scale Biomass Dataset. *ISPRS Annals of the Photogrammetry, Remote Sensing and Spatial Information Sciences*, X-G-2025, 2025. 2

[56] Oriane Siméoni, Huy V. Vo, Maximilian Seitzer, Federico Baldassarre, Maxime Oquab, Cijo Jose, Vasil Khalidov, Marc Szafraniec, Seungeun Yi, Michaël Ramamonjisoa, Francisco Massa, Daniel Haziza, Luca Wehrstedt, Jianyuan Wang, Timothée Darcet, Théo Moutakanni, Leonel Sentana, Claire Roberts, Andrea Vedaldi, Jamie Tolan, John Brandt, Camille Couprie, Julien Mairal, Hervé Jégou, Patrick Labatut, and Piotr Bojanowski. DINov3, 2025. 2, 6, 20

[57] Jong-Chyi Su, Subhransu Maji, and Bharath Hariharan. When does self-supervision improve few-shot learning? In *ECCV*, Berlin, Heidelberg, 2020. Springer-Verlag. 2

[58] Yu Sun, Eric Tzeng, Trevor Darrell, and Alexei A Efros. Unsupervised domain adaptation through self-supervision. *arXiv preprint arXiv:1909.11825*, 2019. 2, 3

[59] Yu Sun, Xiaolong Wang, Liu Zhuang, John Miller, Moritz Hardt, and Alexei A. Efros. Test-Time Training with Self-Supervision for Generalization under Distribution Shifts. In *ICML*, 2020. 2, 3

[60] Mélisande Teng, Amna Elmoustafa, Benjamin Akera, Yoshua Bengio, Hager Radi, Hugo Larochelle, and David Rolnick. SatBird: a Dataset for Bird Species Distribution Modeling using Remote Sensing and Citizen Science Data. In *NIPS*, 2023. 2

[61] Gabriel Tseng, Anthony Fuller, Marlena Reil, Henry Herzog, Patrick Beukema, Favyen Bastani, James R Green, Evan Shelhamer, Hannah Kerner, and David Rolnick. Galileo: Learning Global & Local Features of Many Remote Sensing Modalities. In *ICML*, 2025. 1

[62] Dequan Wang, Evan Shelhamer, Shaoteng Liu, Bruno Olshausen, and Trevor Darrell. Tent: Fully Test-Time Adaptation by Entropy Minimization. In *ICLR*, 2021. 3

[63] Yi Wang, Zhitong Xiong, Chenying Liu, Adam J. Stewart, Thomas Dujardin, Nikolaos Ioannis Bountos, Angelos Zavras, Franziska Gerken, Ioannis Papoutsis, Laura Leal-Taixé, and Xiao Xiang Zhu. Towards a Unified Copernicus Foundation Model for Earth Vision, 2025. 2, 3, 6, 7, 21

[64] Ziquan Wang, Yongsheng Zhang, Zhenchao Zhang, Zhipeng Jiang, Ying Yu, Lei Li, and Lei Zhang. Exploring uncertainty-based self-prompt for test-time adaptation semantic segmentation in remote sensing images. *Remote Sensing*, 16(7), 2024. 3

[65] WEF. Unlocking the potential of earth observation to address africa's critical challenges. Technical report, World Economic Forum, 2021. In collaboration with Digital Earth Africa. 4

[66] Sanghyun Woo, Shoubhik Debnath, Ronghang Hu, Xinlei Chen, Zhuang Liu, In So Kweon, and Saining Xie. ConvNeXt V2: Co-designing and scaling convnets with masked autoencoders. In *Proceedings of the IEEE/CVF conference on computer vision and pattern recognition*, 2023. 20

[67] Zhitong Xiong, Yi Wang, Fahong Zhang, Adam J Stewart, Joëlle Hanna, Damian Borth, Ioannis Papoutsis, Bertrand Le Saux, Gustau Camps-Valls, and Xiao Xiang Zhu. Neural Plasticity-Inspired Foundation Model for Observing the Earth Crossing Modalities. *arXiv preprint arXiv:2403.15356*, 2024. 2, 20

[68] Mouxing Yang, Yunfan Li, Changqing Zhang, Peng Hu, and Xi Peng. Test-time adaptation against multi-modal reliability bias. In *ICLR*, 2024. 3

[69] Eugene Yu Yau, Emily E. Jones, Toby Pak Tsang, Shuang Xing, Richard T. Corlett, Patrick Roehrdanz, David J. Lohman, Adam Kai Lee, Catherine Wai Hai, and Shawan et al. Chowdhury. Spatial occurrence records and distributions of tropical asian butterflies. *Scientific Data*, 12(1004), 2025. 4

[70] Christopher Yeh, Chenlin Meng, Sherrie Wang, Anne Driscoll, Erik Rozi, Patrick Liu, Jihyeon Lee, Marshall Burke, David B. Lobell, and Stefano Ermon. SustainBench: Benchmarks for Monitoring the Sustainable Development Goals with Machine Learning. In *NeurIPS*, 2021. 3

[71] Teresa Yeo, Oğuzhan Fatih Kar, Zahra Sodagar, and Amir Zamir. Rapid Network Adaptation: Learning to Adapt Neural Networks Using Test-Time Feedback. In *ICCV*, 2023. 3

[72] D. Zanaga, R. Van De Kerchove, W. De Keersmaecker, N. Souverijns, C. Brockmann, R. Quast, J. Wevers, A. Grosu, A. Paccini, S. Vergnaud, O. Cartus, M. Santoro, S. Fritz, I. Georgieva, M. Lesiv, S. Carter, M. Herold, Linlin Li, N.E. Tsendbazar, F. Ramoino, and O. Arino. ESA WorldCover 10 m 2020 v100. [doi:10.5281/zenodo.5571936](https://doi.org/10.5281/zenodo.5571936), 2021. 18

[73] Daniele Zanaga, Ruben Van De Kerchove, Wanda De Keersmaecker, Niels Souverijns, Carsten Brockmann, Ralf Quast, Jan Wevers, Alex Grosu, Audrey Paccini, Sylvain Vergnaud, Oliver Cartus, Maurizio Santoro, Steffen Fritz, Ivelina Georgieva, Myroslava Lesiv, Sarah Carter, Martin Herold, Linlin Li, Nandin-Erdene Tsednbazar, Fabrizio Ramoino, and Olivier Arino. ESA WorldCover 10 m 2020 v100, 2021. 4

[74] Shiji Zhao, Shao-Yuan Li, and Sheng-Jun Huang. NanoAdapt: Mitigating Negative Transfer in Test Time Adaptation with Extremely Small Batch Sizes. In *IJCAI. International Joint Conferences on Artificial Intelligence Organization*, 2024. Main Track. 3

[75] Xiao Xiang Zhu, Devis Tuia, Lichao Mou, Gui-Song Xia, Liangpei Zhang, Feng Xu, and Friedrich Fraundorfer. Deep learning in remote sensing: A comprehensive review and list of resources. *IEEE Geoscience and Remote Sensing Magazine*, 2017. 1

# MMEarth-Bench: Global Model Adaptation via Multimodal Test-Time Training

## Supplementary Material

<b>S.1. MMEarth-Bench dataset</b>	<b>12</b>
S.1.1. Overview and format . . . . .	12
S.1.2. Biomass . . . . .	12
S.1.3. Soil Nitrogen, Organic Carbon, & pH . . . . .	14
S.1.4. Species . . . . .	15
S.1.5. Generating tiles . . . . .	17
S.1.6. Dataset splits . . . . .	20
S.1.7. MMEarth-Bench Explorer . . . . .	20
<b>S.2. Practitioner’s guide to using TTT-MMR</b>	<b>20</b>
<b>S.3. Experimental setup</b>	<b>20</b>
S.3.1. Pretrained geospatial models benchmarked . . . . .	20
S.3.2. Modality reconstruction . . . . .	21
S.3.3. TTT-MMR-GEO batching . . . . .	21
S.3.4. Evaluation metrics . . . . .	21
<b>S.4. Additional results</b>	<b>22</b>
S.4.1. Finetuning vs. linear probing . . . . .	22
S.4.2. Test-time training performance with relative improvement metric . . . . .	23
S.4.3. Modality reconstruction visualization . . . . .	24
<b>S.5. Raw results</b>	<b>26</b>
S.5.1. Finetuning . . . . .	26
S.5.2. Joint training and test-time training . . . . .	29
S.5.3. Linear probing . . . . .	30
<b>S.6. Larger figures</b>	<b>33</b>

### S.1. MMEarth-Bench dataset

#### S.1.1. Overview and format

We show the number of tiles in each split for all the MMEarth-Bench tasks in Tab. S.1. We provide information on the modalities in MMEarth-Bench, now including the no-data values, in Tab. S.2. We also display summary statistics for the modalities in Tab. S.3. Summary statistics for the four regression tasks can be found in Tab. S.4 and Tab. S.5. The data for each task dataset is stored in an H5 file, with sizes shown in Tab. S.6. Users can read in data from one of our task H5 files using the code in Fig. S.1. The split data for each task containing the tile indices for the various splits along with the normalization statistics is stored in JSON files. The data is hosted on our [university server](#).

Table S.1. Number of tiles per split by task.

Split	Biomass	Soil N	Soil OC	Soil pH	Species
Train 100%	10665	3787	5359	5711	18882
Train 50%	5332	1894	2680	2856	9441
Train 5%	533	189	268	286	944
Validation	2286	812	1149	1224	4046
Random test	2286	812	1149	1224	4047
Geographic test	3156	232	325	349	9435

#### S.1.2. Biomass

Our biomass dataset is sourced from above-ground biomass measurements collected by NASA’s GEDI mission. To guide our sampling, we divide the planet into its 14 terrestrial biomes, which can be further divided into 846 total ecoregions. The geographic extents of these ecoregions are captured in Google Earth Engine’s [RESOLVE Ecoregions 2017](#) dataset [16]. The GEDI mission only collects data within the latitude band spanning from 51.6° S to 51.6 N, so we do not consider ecoregions outside of this range, leaving 774 remaining. For ecoregions overlapping the boundary of the GEDI range, we crop out the area that does not intersect with the range. We aim to generate 20,000 total biomass tiles. We want the tiles to be distributed approximately evenly across biomes, so we set a target number of tiles per biome given by 1,429, which is the rounded-up quotient of 20,000 tiles divided by 14 biomes. Next, we compute the area of each ecoregion (cropped to the GEDI range) and then sum the areas of the ecoregions within each biome to get the total area of each biome. We then calculate the number of tiles to be generated in each ecoregion by scaling the number of tiles per biome by the fraction of the area the ecoregion covers within its biome and round up to ensure at least 1 tile is generated per ecoregion. This results in 20,421 total tiles. We save this data to a JSON file `ecoregion_tile_counts.json`.

Now we can begin fetching GEDI data from Google Earth Engine. We loop through the biomes and consider the ecoregions one-by-one. We check the number of running SLURM jobs every second and wait to proceed with running the ecoregion until there are maximum 30 jobs running to avoid hitting memory limits on Google Earth Engine. We then submit a 3-day SLURM job with 500MB of RAM and pass in the number of tiles we pre-calculated for the ecoregion.

The process to generate tiles for a given ecoregion is as follows. GEDI L4A is the dataset containing above-ground biomass measurements. We first use Google Earth Engine’s [GEDI L4A table index](#) dataset [18], which contains a list of

Table S.2. **MMEarth-Bench modalities.** Including the number of bands and no-data value for each modality.

Modality	# Bands	Band names	Scale	Type	No-data value
Sentinel-2	12	B1, B2, B3, B4, B5, B6, B7, B8, B8A, B9, B11, B12	Pixel-level	Continuous	65535
Sentinel-1	8	Ascending VV, VH, HH, HV; Descending VV, VH, HH, HV	Pixel-level	Continuous	-9999
ASTER GDEM	2	Elevation, slope	Pixel-level	Continuous	-9999
ETH Global Canopy Height	2	Height, uncertainty	Pixel-level	Continuous	255
Dynamic World	1	Landcover	Pixel-level	Categorical	9
ESA WorldCover	1	Landcover	Pixel-level	Categorical	11
Precipitation	3	Previous month, month, year	Tile-level	Continuous	-9999
Temperature	9	Previous month max, mean, min; Month max, mean, min; Year max, mean, min	Tile-level	Continuous	-9999
Geolocation	2	Longitude, latitude	Tile-level	Continuous	N/A
Sentinel-2 date	1	Date	Tile-level	Continuous	N/A
Biome	1	Biome number	Tile-level	Categorical	14
Ecoregion	1	Ecoregion number	Tile-level	Categorical	846

Table S.3. **Modality statistics.** NaN percentage and [min, max] range across all tasks.

Modality	Biomass		Soil Nitrogen		Soil Organic Carbon		Soil pH		Species	
	NaN %	[Min, Max]	NaN %	[Min, Max]	NaN %	[Min, Max]	NaN %	[Min, Max]	NaN %	[Min, Max]
Sentinel-2	1.79e-03%	[0.00, 2.07e+04]	9.84e-04%	[0.00, 1.81e+04]	1.63e-03%	[0.00, 2.03e+04]	9.28e-04%	[0.00, 2.03e+04]	7.88e-04%	[0.00, 2.27e+04]
Sentinel-1	6.08e+01%	[-70.29, 31.73]	6.12e+01%	[-64.31, 32.83]	6.19e+01%	[-64.31, 37.43]	6.11e+01%	[-64.31, 37.43]	5.68e+01%	[-75.43, 29.50]
ASTER GDEM elevation	0.0%	[-186.35, 6117.91]	0.0%	[-32.49, 5557.40]	0.0%	[-32.49, 5557.40]	0.0%	[-31.00, 5557.40]	0.0%	[-427.00, 6649.21]
ASTER GDEM slope	0.0%	[0.00, 77.56]	0.0%	[0.00, 78.61]	0.0%	[0.00, 77.77]	0.0%	[0.00, 78.61]	0.0%	[0.00, 79.94]
ETH GCH height	1.48%	[0.00, 59.96]	1.70%	[0.00, 64.00]	2.33%	[0.00, 60.00]	1.85%	[0.00, 64.00]	2.74%	[0.00, 68.34]
ETH GCH uncertainty	1.48%	[0.00, 246.00]	1.70%	[0.00, 252.00]	2.33%	[0.00, 252.00]	1.85%	[0.00, 252.00]	2.74%	[0.00, 253.00]
Dynamic World	1.03%	[0.00, 8.00]	4.07e-02%	[0.00, 8.00]	4.17e-02%	[0.00, 8.00]	3.19e-02%	[0.00, 8.00]	3.02e-01%	[0.00, 8.00]
ESA WorldCover	0.0%	[0.00, 10.00]	0.0%	[0.00, 10.00]	2.51e-02%	[0.00, 10.00]	2.35e-02%	[0.00, 10.00]	0.0%	[0.00, 10.00]
Precipitation	1.54%	[1.80e-05, 12.07]	1.22%	[1.80e-05, 7.33]	1.01%	[1.80e-05, 5.60]	7.17e-01%	[1.80e-05, 7.33]	9.23e-01%	[1.80e-05, 10.91]
Temperature	1.54%	[227.58, 324.67]	1.22%	[220.34, 320.92]	1.01%	[220.34, 320.92]	7.17e-01%	[220.34, 320.92]	9.23e-01%	[218.25, 326.06]
Geolocation	0.0%	[-179.97, 179.60]	0.0%	[-160.03, 175.45]	0.0%	[-161.96, 175.45]	0.0%	[-160.03, 172.73]	0.0%	[-179.89, 179.81]
Geolocation encoding	0.0%	[-1.00, 1.00]	0.0%	[-1.00, 1.00]	0.0%	[-1.00, 1.00]	0.0%	[-1.00, 1.00]	0.0%	[-1.00, 1.00]
Month encoding	0.0%	[-1.00, 1.00]	0.0%	[-1.00, 1.00]	0.0%	[-1.00, 1.00]	0.0%	[-1.00, 1.00]	0.0%	[-1.00, 1.00]
Biome	0.0%	[0.00, 13.00]	4.08e-01%	[0.00, 12.00]	3.01e-01%	[0.00, 13.00]	1.18e-01%	[0.00, 13.00]	8.18e-01%	[0.00, 13.00]
Ecoregion	0.0%	[3.00, 845.00]	4.08e-01%	[2.00, 828.00]	3.01e-01%	[2.00, 844.00]	1.18e-01%	[2.00, 844.00]	8.18e-01%	[2.00, 843.00]
MSK CLDPRB	0.0%	[0.00, 100.00]	0.0%	[0.00, 100.00]	0.0%	[0.00, 100.00]	0.0%	[0.00, 100.00]	0.0%	[0.00, 100.00]
S2CLOUDLESS	0.0%	[0.00, 100.00]	0.0%	[0.00, 100.00]	0.0%	[0.00, 100.00]	0.0%	[0.00, 100.00]	0.0%	[0.00, 100.00]
SCL	1.47e-04%	[2.00, 11.00]	4.11e-04%	[2.00, 11.00]	3.92e-04%	[2.00, 11.00]	1.46e-04%	[2.00, 11.00]	3.14e-04%	[2.00, 11.00]
MSK CLDPRB CLOUDY PIXEL FRACTION	0.0%	[0.00, 0.18]	0.0%	[0.00, 0.16]	0.0%	[0.00, 0.17]	0.0%	[0.00, 0.17]	0.0%	[0.00, 0.23]
S2CLOUDLESS CLOUDY PIXEL FRACTION	0.0%	[0.00, 0.19]	0.0%	[0.00, 0.17]	0.0%	[0.00, 0.17]	0.0%	[0.00, 0.17]	0.0%	[0.00, 0.17]
SCL NO DATA PIXEL FRACTION	0.0%	[0.00, 0.02]	0.0%	[0.00, 0.02]	0.0%	[0.00, 0.02]	0.0%	[0.00, 0.01]	0.0%	[0.00, 0.04]

Table S.4. **Split statistics for regression tasks.** Values are mean  $\pm$  standard deviation. Units are Mg/ha for biomass and g/kg for soil N and soil OC.

Split	Biomass	Soil N	Soil OC	Soil pH
Train 100%	$62.51 \pm 99.24$	$4.98 \pm 6.08$	$81.21 \pm 125.10$	$6.10 \pm 1.32$
Train 50%	$63.86 \pm 102.75$	$5.01 \pm 6.11$	$81.77 \pm 126.70$	$6.10 \pm 1.33$
Train 5%	$61.09 \pm 101.79$	$4.47 \pm 5.99$	$75.40 \pm 128.10$	$6.18 \pm 1.35$
Validation	$63.80 \pm 101.03$	$4.97 \pm 6.42$	$81.67 \pm 123.34$	$6.08 \pm 1.32$
Random test	$65.14 \pm 99.81$	$4.66 \pm 6.08$	$74.72 \pm 111.76$	$6.12 \pm 1.30$
Geographic test	$26.09 \pm 66.16$	$3.03 \pm 4.97$	$25.38 \pm 43.25$	$6.59 \pm 1.24$

the GEDI L4A collection IDs along with their start and end times. We only consider data from the year 2020, so we filter the list to include only those collections that have data in 2020. We then extract the geographic range of the ecoregion cropped to the GEDI range as discussed earlier. We use this

Table S.5. **Split ranges for regression tasks.** Values are [min, max]. Units are Mg/ha for biomass and g/kg for soil N and soil OC.

Split	Biomass	Soil N	Soil OC	Soil pH
Train 100%	[0.00, 1991.21]	[0.00, 38.81]	[0.00, 779.00]	[3.00, 10.70]
Train 50%	[0.00, 1991.21]	[0.00, 38.80]	[0.00, 779.00]	[3.00, 10.70]
Train 5%	[0.00, 1794.24]	[0.04, 38.80]	[0.00, 779.00]	[3.40, 9.50]
Validation	[0.00, 1981.19]	[0.00, 69.07]	[0.00, 630.30]	[3.20, 10.00]
Random test	[0.00, 1991.65]	[0.00, 33.86]	[0.00, 650.00]	[3.00, 9.90]
Geographic test	[0.67, 1975.70]	[0.07, 33.70]	[0.30, 422.80]	[3.60, 10.30]

ecoregion range to filter the table index dataset to yield only those collections that have data for the desired ecoregion in the year 2020. We then create a list of their collection IDs and query the collections that are valid assets. We merge all these collections into a single collection. We then fil-

```

import h5py
import json

with h5py.File(PATH_TO_H5, 'r') as h5_file:
    if KEY in ['sentinel2_date', 'crs', 'sentinel2_system_index']:
        key_data = h5_file[KEY].asstr()[...]
    elif KEY in ['missing_modalities', 'species']:
        key_data = [json.loads(lst) for lst in h5_file[KEY].asstr()[...]]
    elif KEY in ['Sentinel2', 'Sentinel1', 'ASTER_GDEM', 'ETH_GCH', 'DynamicWorld', \
                 'ESA_WorldCover', 'precipitation', 'temperature', 'geolocation_encoding', \
                 'month_encoding', 'biome', 'ecoregion', 'biomass', 'soil_nitrogen', \
                 'soil_organic_carbon', 'soil_pH', 'MSK_CLDPRB', 'S2CLOUDLESS', 'SCL', \
                 'geolocation', 'MSK_CLDPRB_CLOUDY_PIXEL_FRACTION', \
                 'S2CLOUDLESS_CLOUDY_PIXEL_FRACTION', 'SCL_NO_DATA_PIXEL_FRACTION', 'id', \
                 'transform']:
        key_data = h5_file[KEY] [:]

```

Figure S.1. **Python code for reading data from H5 files in MMEarth-Bench.** Both modalities and tasks can be provided as keys.

Table S.6. **Data volume.** One H5 file per task. Size recorded in gigabytes (G).

Biomass	Soil N	Soil OC	Soil pH	Species
16.0G	4.3G	6.0G	6.4G	28.0G

ter the collection by the bounds of the ecoregion to exclude GEDI points outside of the ecoregion. We then apply quality filters to only keep points that have “degrade\_flag = 0,” “l2\_quality\_flag = 1,” “l4\_quality\_flag = 1,” “leaf\_off\_flag = 0” (growing season) and “region\_class > 0” (land). We then apply a filter to only keep points whose leaf-off day is after their leaf-on day. This is to make it more straight-forward to generate a leaf-on date filter later on when downloading the data modalities. Finally, we filter by GEDI points with biomass value  $\leq 2,000$  since the plots in Duncanson et al. [19] only show AGBD values up to  $\approx 2,000$ .

Next, we randomly shuffle the GEDI points and select however many points are needed from the beginning of the list, possibly fewer depending on how many there are. We then export the collection of points to a bucket in Google Cloud Storage in GeoJSON format. Once it has been uploaded, we download the file. If there is at least one point in the collection, we generate an outer tile around each point of size 1,300x1,300-m. The outer tile is larger than our desired tile by one pixel on each side. We do this because later on we construct the tile on the Sentinel-2 grid, and because in that grid a single pixel spans 10m across, our resultant tile could be shifted from our original intended tile by a maximum of 1 pixel or 10m in each direction. Hence we make an “outer tile” that is guaranteed to contain our final tile for the purpose of checking overlap between tiles. We then remove points with overlapping tiles and shuffle those

remaining. We then select the number of points we need from the start of the list, possibly fewer depending on if we lost some points due to overlap removal. If the number of points is equal to the number of desired ecoregion tiles or the number of points before removing overlaps was less than the number of ecoregion tiles, we save the points’ data as a GeoJSON. Otherwise, we select twice however many points are needed from the shuffled list of GEDI points and repeat the above process. If there are still not enough points, then we select three times however many points are needed and continue this loop until there are enough points left over after removing overlaps. We then merge all of the ecoregion points into a single list, remove any overlaps among points from all the ecoregions, and then save the remaining points as a single GeoJSON file containing 19,834 points. Note that this is 587 points fewer than our intended 20,421. This is because 14 ecoregions had 0 GEDI points when 1 was desired and one ecoregion had only 38 GEDI points when 578 were desired. Finally, we concatenate all the points from all the ecoregions. The biomass point generation process took  $\approx 50$  hours. The points list is then shuffled and each point is assigned an ID. Figure S.2a shows how many points are missing each of the modalities after generating tiles. Figure S.3a visualizes the distribution in biomass values across the train, validation, random test, and geographic test sets.

### S.1.3. Soil Nitrogen, Organic Carbon, & pH

Our soil datasets are sourced from the [WoSIS December 2023 snapshot](#) [7]. We consider the datasets for nitrogen, organic carbon, and pH. [SoilGrids](#), a model that predicts soil properties based on environmental covariates, exhibited a decrease in performance with increasing soil depth due to a weaker relationship between environmental covariates and soil properties in the deeper layers [48]. Thus, we filter

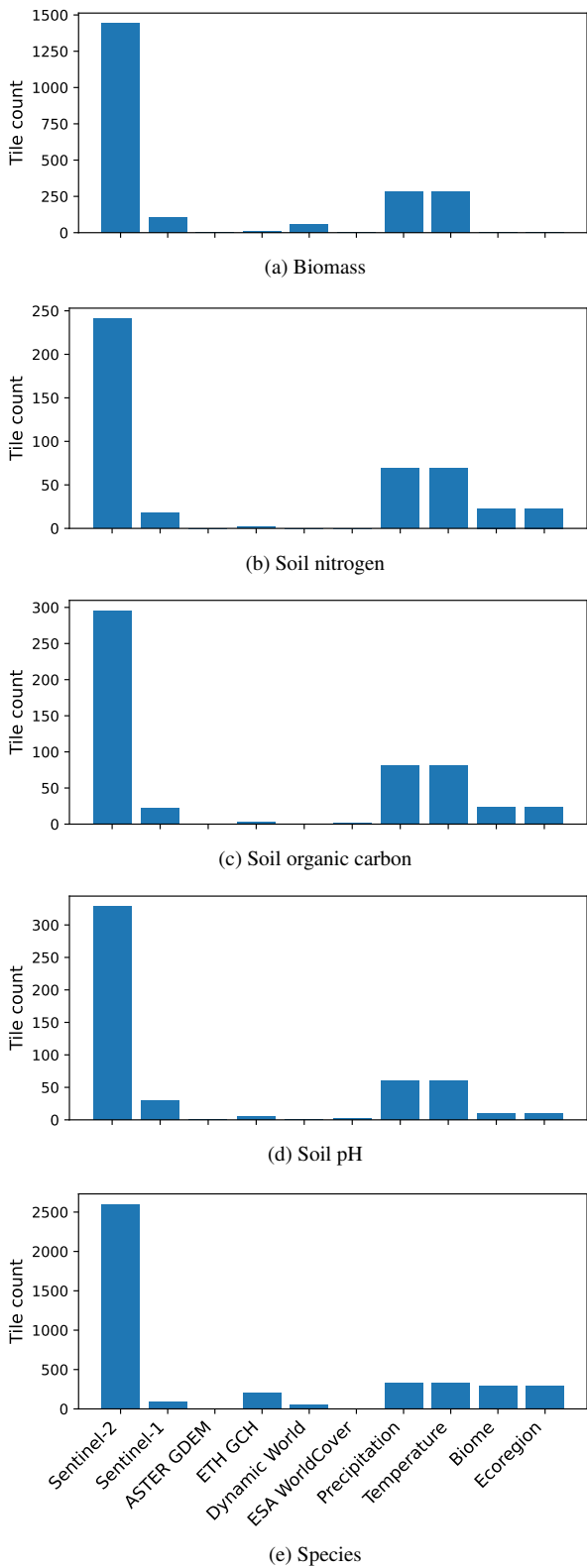


Figure S.2. **Missing modality counts per task.** When downloading modality data from GEE for the tiles, we record which modalities are missing. If Sentinel-2 was missing, we did not save the tile or attempt to download the rest of the modalities.

the three datasets by measurements within the depth range 0-5 cm, which is the shallowest soil layer of the six standard layers defined in the [GlobalSoilMap](#) specifications [2]. We then filter measurements by those whose positional uncertainty is “circa 100 m,” which is the strictest option. We then save the remaining points along with their outer tiles and “value\_avg”. This results in 8,991 soil nitrogen points, 11,593 soil organic carbon points, and 12,283 soil pH points. For each task, we shuffle the points, remove overlaps among the outer tiles as we did for biomass, assign an ID to each point, and then save the data to a GeoJSON. This yields 5,884 points for soil nitrogen, 8,277 points for soil organic carbon, and 8,836 points for soil pH.

Figures S.2b to S.2d show how many points are missing each of the modalities for the three soil tasks after generating tiles. Figures S.3b to S.3d visualize the distribution in soil nitrogen, organic carbon, and pH values, respectively, across the train, validation, random test, and geographic test sets.

#### S.1.4. Species

Our species data is sourced from the terrestrial mammals polygon shapefile, which is one of the data products on the [IUCN Red List’s Spatial Data Download](#) page [1]. The data we use comes from Version 2025-1, last updated on March 27, 2025. We downloaded the data on June 13, 2025. We later use Africa as our geographic held-out test region, so we need to ensure that our selected species occur both in and out of Africa. We use the QGIS software to draw a Polygon representing Africa for the purpose of our geographic split. We base our boundary on the [Tectonic Plate Boundaries KMZ](#) file provided by the USGS [49] as well as Esri’s [World Continents](#) GeoJSON available on ArcGIS Hub [20]. We export our Africa polygon as a GeoJSON.

The terrestrial mammals shapefile has a row for each disjoint part of a species’ range. We dissolve the GeoDataFrame by species name so that each row corresponds to a unique species and the multiple Polygons per species are combined into a single MultiPolygon. This results in 5,675 rows. We then filter the GeoDataFrame by species whose range intersects with Africa, leaving 1,451 species. We then reproject the species GeoDataFrame and the Africa geometry to EPSG:6933, the global equal area projection. In this projection, we compute for each species how much of its range is in and outside Africa in square kilometers. There are 122 species with nonzero area both in and outside Africa. We then filter by species whose range covers at least 6,000 km<sup>2</sup> both in and outside Africa, leaving 101 species. We take the first 100 in the list. Of these final 100 selected species, the minimum area in Africa is 12,018.38 km<sup>2</sup> and the minimum area outside Africa is 6,218.04 km<sup>2</sup>. We save the ranges of these 100 species to a GeoJSON. Figure S.4 shows the taxonomic orders of the selected species.

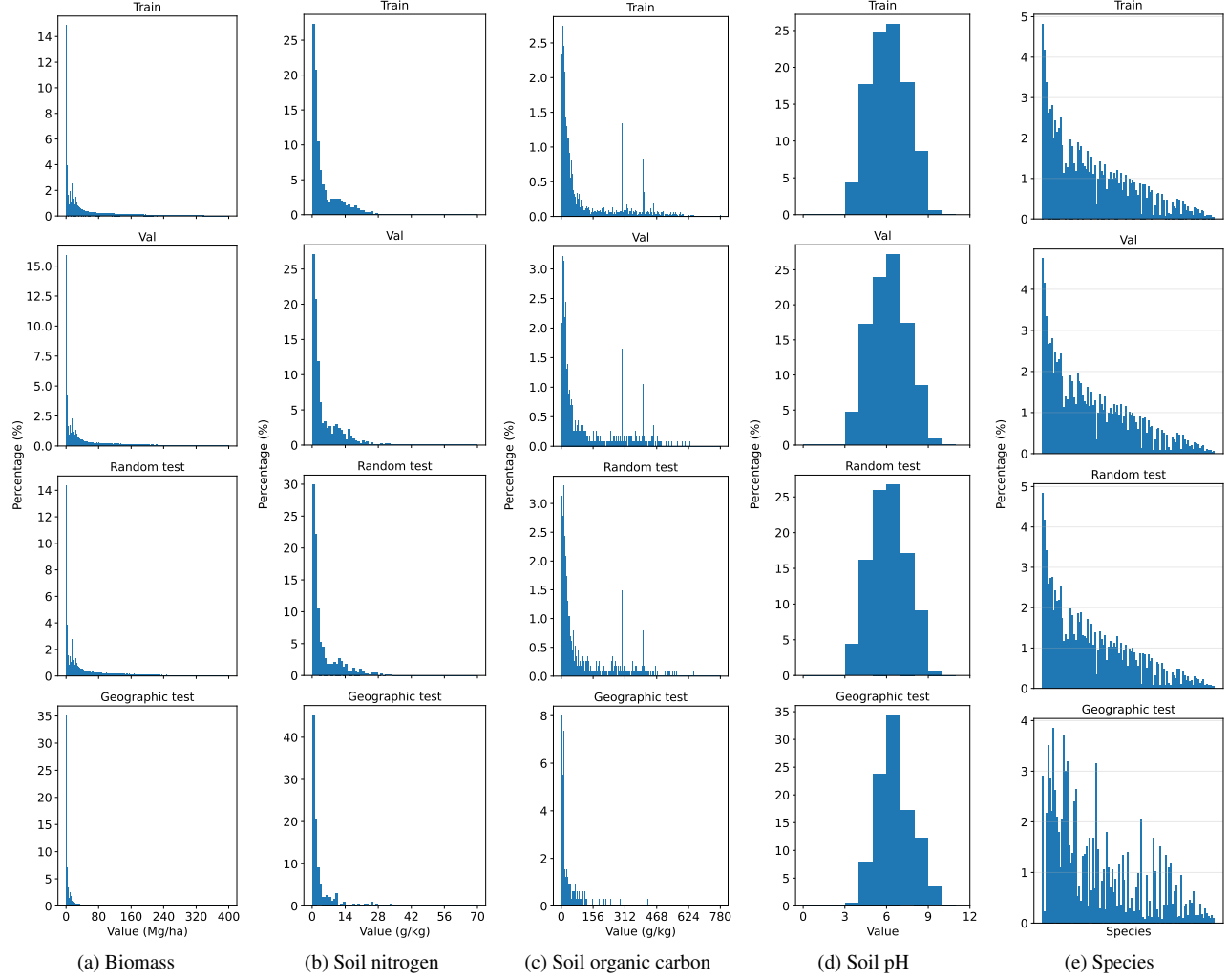


Figure S.3. **Distributions across splits for MMEarth-Bench tasks.** The species are ordered as in Fig. S.5.

Now, we need to generate points from these species ranges. For each row in the GeoDataFrame we just created, we extract the species name as well as its range in and out of Africa using the GeoJSON for the boundary of Africa we made before. We aim to generate 100 points in Africa and 300 out of Africa. We first extract the bounding box of the range in Africa. We then uniformly randomly pick  $x$  and  $y$  coordinates within the bounding box. We create a point from these coordinates with an outer tile. If the outer tile intersects the species' range in Africa, we save the point to a list along with the name of the species and its outer tile. We continue generating coordinates until we have points for the species in Africa. This same process is then repeated for outside Africa. Afterwards, we combine the in-Africa and out-of-Africa points into a single list and remove overlaps among them. We append this list to an overall list of points. When this process has been completed

for all species, our overall list has 39,676 points. We remove overlaps among all of those, resulting in 39,011 points. We then loop through each point in this list and check whether its outer tile overlaps with any of the other species' ranges. If so, we add the species to the point's species list. Finally, we shuffle the points and assign them IDs before saving the data to a GeoJSON. The maximum and minimum numbers of points per species are 35,468 and 530, respectively.

Figure S.2e shows how many points are missing each of the modalities after generating tiles. The maximum and minimum numbers of tiles per species are 32,982 and 525, respectively. We assign each species a distinct integer label from 0-99 to be used during modeling. The minimum number of tiles in which a species appears by split is 187 for train, 32 for validation, 46 for random test, and 173 for geographic test. Fig. S.5 shows how many tiles each species occurs in, and Fig. S.6 plots how many tiles contain a cer-

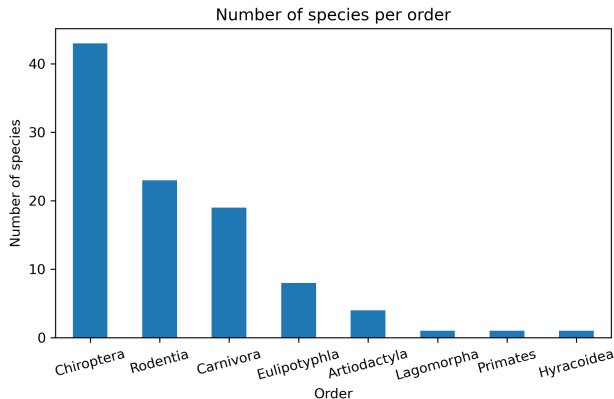


Figure S.4. Species distribution per taxonomic order.

tain number of species.

### S.1.5. Generating tiles

Once we have saved the GeoJSONs containing the coordinates of all the points, we are ready to generate tiles with paired modalities and task data. For a given task, for each point, we first need to determine a date range to be used for filtering modality data. For biomass, we first extract the GEDI points within the point's outer tile following the same procedure as described earlier. Then, we extract each GEDI point's leaf-on and leaf-off day and create a list with unique pairs of (leaf-on, leaf-off) days. We then convert each integer day into a valid date format. The date filter to be used is then any date that falls within any of those date ranges, corresponding to a leaf-on time period. For the soil and species tasks, we estimate the growing season by using the months May-September for northern-hemisphere points and November-March for southern-hemisphere points and use that as the date filter. We generate a 1280x1280-m tile centered on the point by applying a buffer.

#### S.1.5.1. Sentinel-2

We obtain Sentinel-2 images from the [Harmonized Sentinel-2 MSI: MultiSpectral Instrument, Level-2A](#) dataset on Google Earth Engine. We first filter by the pre-selected date range to extract all images with a valid date. Then we filter by images that have some overlap with the tile. We then apply a stricter filter to ensure that we only keep images that contain the tile plus a 200-m buffer to avoid edge effects. If no images pass all the filters, then we do not include the point in the resulting dataset. If at least one image did pass the filters, we use the MSK\_CLDPRB band to compute a cloudy pixel fraction for each image within the tile, where we define a cloudy pixel as one with  $\geq 10\%$  cloud probability. We then filter to only keep im-

ages with  $< 10\%$  cloudy pixels. We again check if any images have passed the filter and skip over the point if none have. If there is at least one image left, we apply a second cloud filter using the [Sentinel-2: Cloud Probability](#) dataset from Google Earth Engine. We apply the same three filters as above. We then save the data as an additional band for each of the images, using the "system:index" value for pairing. We then use this S2CLOUDLESS band to compute another cloudy pixel fraction, again using 10% as the threshold for classifying a pixel as cloudy and filtering by images with  $< 10\%$  cloudy pixels. We again skip over the point if no images have passed the filter. If there are some left, we then apply a filter against invalid pixels using the SCL band in Sentinel-2 images. We only keep images that have less than 10% no-data pixels in the SCL band. We then sort the images in ascending order by their fraction of no-data SCL pixels and take the one with the lowest value. We once again skip over the point if no images have passed the filter. We access the date property of the image, the projection of the B4 band, and the CRS of the B4 band. We then project the coordinates of the tile using that projection and round the coordinates to land on the nearest pixel intersection. We then set the tile to be the 128x128-pixel square centered at that pixel intersection. We then apply a bilinear projection to the bands in the image with continuous pixel values and unmask to the Sentinel-2 no-data value of 65,535. We apply a nearest-neighbor projection to SCL which has categorical pixel values and unmask it to 0, which was its original no-data value. We then save the data for all of the bands. We save B1, B2, B3, B4, B5, B6, B7, B8, B8A, B9, B11, and B12 as our Sentinel-2 modality bands, and we also save MSK\_CLDPRB, S2CLOUDLESS, and SCL as additional metadata. This results in a 12-band continuous-valued modality.

#### S.1.5.2. Sentinel-1

We obtain Sentinel-1 images from the [Sentinel-1 SAR GRD: C-band Synthetic Aperture Radar Ground Range Detected, log scaling](#) dataset on Google Earth Engine. We apply the same three filters as for Sentinel-2 and also filter by images with the interferometric wide swath mode. We then calculate the difference between the date of each image and the date of the Sentinel-2 image we selected. We sort the images in ascending order by how many days off they are from the Sentinel-2 image date. We extract all the ascending images and then take the first one. We also extract all the descending images and then take the first one. For both the ascending and descending image, we save the VV, VH, HH, and HV bands bilinearly projected to match Sentinel-2 if they exist, otherwise we save them as a NaN band using the Sentinel-1 no-data value of -9,999. We also unmask the image to the Sentinel-1 no-data value. This results in an 8-band continuous-valued modality. If there is neither an ascending nor descending image, we mark the modality as

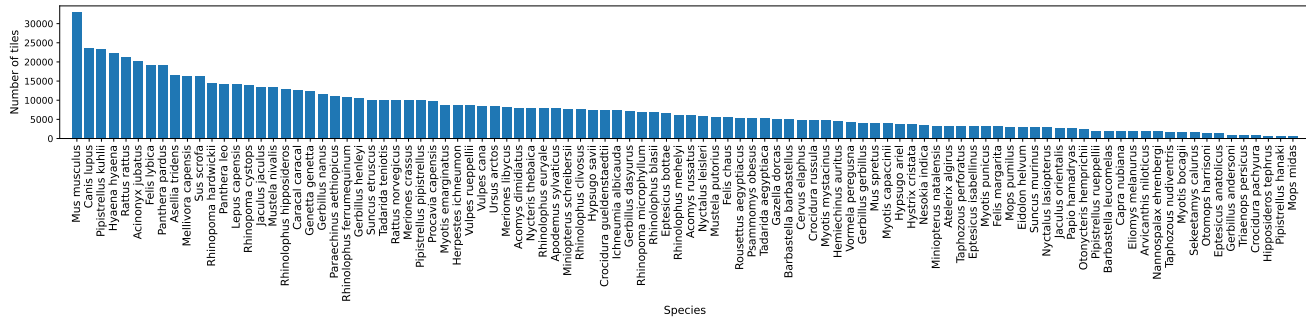


Figure S.5. **Species occurrence across all tiles.** Multiple species can be present per tile.

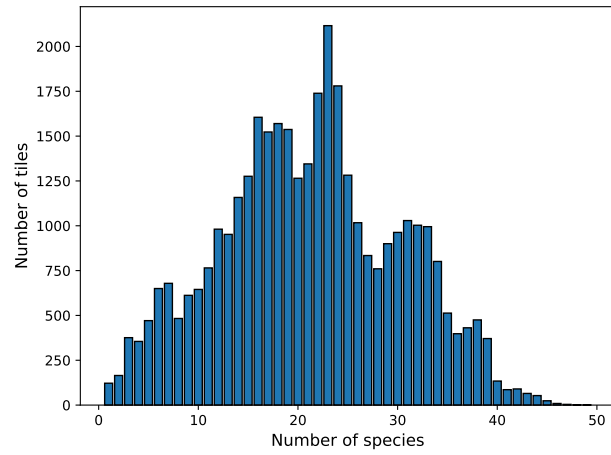


Figure S.6. **Species richness per tile.** Visualization of how many tiles contain each number of species. For example, we see that 23 is the most common number of species to occur in a tile, making this a strongly multi-label task.

missing.

### S.1.5.3. ASTER GDEM

We access elevation data from the GDEM dataset within the sat-io Aster data available on Google Earth Engine. We mask no-data values and then calculate the slope from the elevation data. We then bilinearly project both the elevation and slope bands and unmask them to the no-data value. This results in a 2-band continuous-valued modality. If all the pixels in the elevation band are no-data, we mark the modality as missing.

### S.1.5.4. ETH Global Canopy Height

We access canopy height data from the ETH Global Canopy Height 2020 10m map [31] available on Google Earth Engine. We use both the height and uncertainty bands, bilinearly reproject them, and unmask to the original no-data value of 255 for the product, resulting in a 2-band continuous-valued modality. If all the pixels in the height

band are no-data, we mark the modality as missing.

### S.1.5.5. Dynamic World

We obtain Dynamic World data from the [Dynamic World V1](#) collection on Google Earth Engine, which has 9 land-cover classes [11]. We filter by images within 2020 and those that have some overlap with the selected tile. We then get the mode for each pixel across images and use that as our image. If no image was found, we create a constant-valued image filled with the no-data value of 9 and reproject it using nearest-neighbor resampling. Otherwise, we reproject the image we obtained and unmask it to the no-data value. This yields a 1-band categorical-valued modality. If all the pixels in the image are no-data, we mark the modality as missing.

### S.1.5.6. ESA WorldCover

We obtain ESA WorldCover data from the [ESA WorldCover 10m v100](#) collection on Google Earth Engine, which has 11 landcover classes [72]. We remap the class labels such that  $10 \rightarrow 0$ ,  $20 \rightarrow 1$ ,  $30 \rightarrow 2$ ,  $40 \rightarrow 3$ ,  $50 \rightarrow 4$ ,  $60 \rightarrow 5$ ,  $70 \rightarrow 6$ ,  $80 \rightarrow 7$ ,  $90 \rightarrow 8$ ,  $95 \rightarrow 9$ , and  $100 \rightarrow 10$ . We project the image using nearest-neighbor resampling and unmask it to the no-data value of 11, yielding a 1-band categorical-valued modality. If all the pixels in the image are no-data, we mark the modality as missing.

### S.1.5.7. Precipitation & Temperature

We obtain precipitation and temperature data from the [ERA5-Land Monthly Aggregated - ECMWF Climate Reanalysis](#) dataset on Google Earth Engine. We collect temperature mean, min, and max as well as total precipitation data for the month corresponding to the Sentinel-2 image, the month prior, and the year ending with the selected month. This data already exists at the month-level and we compute it at the year-level. For each band (3 for precipitation and 9 for temperature), we compute the mean over the tile. If the value is None, then we instead use the no-data value of -9,999. This results in a 3-band continuous-valued modality for precipitation and a 9-band continuous-valued modality for temperature.

### S.1.5.8. Geolocation

We extract the longitude and latitude of the centroid of the tile that has been snapped to the Sentinel-2 grid, yielding a 2-band continuous-valued modality. We also compute a geolocation encoding:

$$[\cos(\text{lon}), \sin(\text{lon}), \cos(\text{lat}), \sin(\text{lat})].$$

### S.1.5.9. Sentinel-2 date

We save the date of the selected Sentinel-2 image as a string in YYYY-MM-dd format, yielding a 1-band continuous-valued modality. We also extract the month from this date and compute a month encoding by  $[\cos(\pi \times \text{month}/6), \sin(\pi \times \text{month}/6)]$ .

### S.1.5.10. Biome & Ecoregion

We store the biome and ecoregion names along with their corresponding numbers in `biome_labels.json` and `ecoregion_labels.json`, respectively. We access the same ecoregions dataset as before and filter it by the centroid of the final tile. We then extract the biome and ecoregion information from that if it is available. If it is, we map each biome name to an integer in 0-12 and each ecoregion name to an integer in 0-845 using the JSONs mentioned above. If the biome information is not available, we set biome to the no-data value of 13. If the ecoregion information is not available, we set ecoregion to the no-data value of 846. This results in a 1-band categorical-valued modality for biomass and a 1-band categorical-valued modality for ecoregion.

### S.1.5.11. Task Data

We must also include the data for each task in the tiles. For biomass, we initialize a NaN image with -9,999 constant values and then write over it with the GEDI points we extracted for the tile. We reproject this to match the Sentinel-2 grid with nearest-neighbor resampling. For the soil properties, we save the value of the property together with the point in the GeoJSON, so we simply read in that value. For species, we save the list of species present in the tile together with the point in the GeoJSON, so we can simply read in that list.

### S.1.5.12. Saving Data

All modalities except for geolocation and date could in theory be unavailable for a tile. In Figure S.2, we visualize how many tiles for each task have missing modalities. If Sentinel-2 was missing, we did not save the tile. The data for all the other tiles is downloaded and saved as a TIFF. Each TIFF contains an array of shape (29,128,128) except for biomass, which has an additional band for the biomass data, yielding shape (30,128,128). The band names are shown in Table S.7. Each TIFF also has a dictionary of tags containing the tile-level data (tile-level modalities along with the geolocation encoding, month

Table S.7. **TIFF band indices and names.** Note that Band 29 “biomass” is only present for the biomass task.

Band index	Band name
0	Sentinel2_B1
1	Sentinel2_B2
2	Sentinel2_B3
3	Sentinel2_B4
4	Sentinel2_B5
5	Sentinel2_B6
6	Sentinel2_B7
7	Sentinel2_B8
8	Sentinel2_B8A
9	Sentinel2_B9
10	Sentinel2_B11
11	Sentinel2_B12
12	MSK_CLDPRB
13	S2CLOUDLESS
14	SCL
15	Sentinel1Ascending_VV
16	Sentinel1Ascending_VH
17	Sentinel1Ascending_HH
18	Sentinel1Ascending_HV
19	Sentinel1Descending_VV
20	Sentinel1Descending_VH
21	Sentinel1Descending_HH
22	Sentinel1Descending_HV
23	ASTER_GDEM_elevation
24	ASTER_GDEM_slope
25	ETH_GCH_height
26	ETH_GCH_uncertainty
27	DynamicWorld
28	ESA_WorldCover
29	biomass

encoding, missing modalities, MSK\_CLDPRB cloudy pixel fraction, S2CLOUDLESS cloudy pixel fraction, SCL no data fraction, and task value if the task is not biomass). The TIFF file also contains the tile ID, CRS, and transform. We save TIFFs for all tiles we can generate and then merge the TIFFs into a single H5 file for each task. The keys in the H5 file are Sentinel2, Sentinel1, ASTER\_GDEM, ETH\_GCH, DynamicWorld, ESA\_WorldCover, precipitation, temperature, geolocation, sentinel2\_date, biome, ecoregion, geolocation\_encoding, month\_encoding, MSK\_CLDPRB, MSK\_CLDPRB\_CLOUDY\_PIXEL\_FRACTION, S2CLOUDLESS, S2CLOUDLESS\_CLOUDY\_PIXEL\_FRACTION, SCL, SCL\_NO\_DATA\_PIXEL\_FRACTION, crs, id, missing\_modalities, transform, sentinel2\_system\_index, and task, where “task” is the name of the task. Sentinel-2 system index uniquely identifies the Sentinel-2 image used

for each tile.

### S.1.6. Dataset splits

We split each task dataset into a train set, validation set, random test set, and geographic test set. We use the tiles in Africa as the geographic test set, and we randomly split the tiles in the rest of the world into train, validation, and random test sets with ratios 70%/15%/15%.

We do this by first extracting the bounding box for each tile and reprojecting it into EPSG 4326. Each tile is also assigned an index. We split these boxes into an Africa group and a non-Africa group. The Africa group contains all tiles that intersect our Africa polygon, and the non-Africa group contains the rest. We randomly shuffle the non-Africa tiles and then assign the first 70% for training, the next 15% for validation, and the remaining 15% for random testing. We calculate normalization statistics on the training tiles for the Sentinel-2, Sentinel-1, ASTER GDEM, ETH GCH, precipitation, and temperature modalities. In particular, we mask out the no-data value for each modality and then compute the mean and standard deviation for each band. We save the task’s train, validation, and random test indices along with the normalization statistics to a JSON file.

### S.1.7. MMEarth-Bench Explorer

We have developed an interactive map visualization tool available at <https://lgordon99.github.io/mmearth-bench-app/> to visualize the MMEarth-Bench dataset. The app was made with HTML, CSS, and JavaScript and runs in the browser. We show selected screenshots in Fig. S.7.

## S.2. Practitioner’s guide to using TTT-MMR

Our test-time training method is not limited to the MMEarth-Bench tasks. Others wishing to adapt a pre-trained model to their downstream task can extract the MMEarth modalities using our code and then run JT followed by TTT-MMR in order to get more accurate predictions. Downloading the MMEarth modalities requires a GeoJSON of (lon, lat) coordinates for the task data. See Fig. S.8 for an example. This GeoJSON should be accessible at a path such as `DATA_DIR/TASK/TASK_points.geojson`. The modalities can then be downloaded using `python get_tile_data.py TASK`.

Our TTT approach takes <1 sec/sample at inference time, making it highly usable for practitioners (Tab. S.8). With <10k samples per test set, it takes maximum 2.5 hours on a single GPU.

	DINOv3 Sat	MPMAE	Copernicus-FM
Standard forward pass	0.007	0.002	0.009
TTT-MMR-GEO (5 iters)	0.910	0.367	0.706

Table S.8. Compute time for inference (seconds/sample)

## S.3. Experimental setup

### S.3.1. Pretrained geospatial models benchmarked

#### S.3.1.1. RGB input

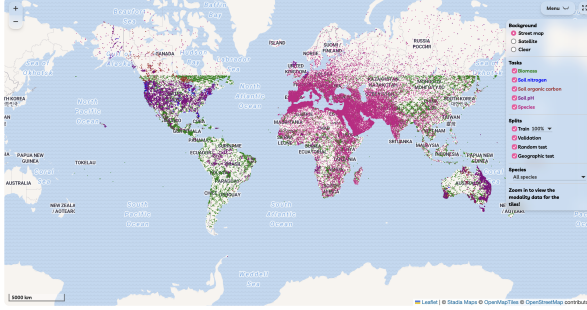
Scale-MAE [51] pretrains a ViT-L model according to the masked autoencoding framework with the addition of a ground sampling distance (GSD) positional encoding. They pretrain on the fMoW-RGB [13] dataset, which contains remotely sensed images of varying resolution and GSD. DINOv3 [56] trains a 7B-parameter DINO model, a variant of the ViT architecture, with the new Gram anchoring strategy to remove noise from the feature maps. Subsequently, this model is distilled into smaller models, such as ViT-L. We benchmark DINOv3 Web, the ViT-L distilled from the 7B-parameter model pretrained on the web imagery dataset LVD-1689M [56], and DINOv3 Sat, the ViT-L distilled from the 7B-parameter model pretrained on their SAT-493M dataset [56] derived from Maxar RGB images.

#### S.3.1.2. Sentinel-2 input

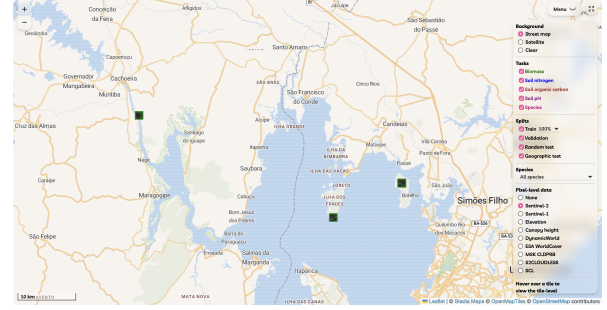
SatlasNet [6] contains a Swin Transformer backbone and separate heads for different label types (e.g., segmentation or point). They train both multi-image (time series) and single-image models. All models are pretrained on SatlasPretrain [6], a dataset of 856K tiles with an associated time series of remote sensing imagery of varying resolution (Sentinel-2 and NAIP) and labels drawn from 137 categories. We benchmark the single-image (9-band) Sentinel-2 pretrained Swin-v2-B backbone. MPMAE [42] is a multi-pretext masked autoencoder approach to training a ConvNeXtV2-based architecture [66]. They pretrain in a self-supervised manner on multimodal pretext tasks using the data in the MMEarth dataset [42] in order to learn semantic representations for Sentinel-2, the model’s input. The MMEarth pretraining dataset contains the same modalities as our MMEarth-Bench. We benchmark their attosized model that was pretrained on MMEarth64 with an uncertainty-weighted loss on  $56 \times 56$ -pixel images.

#### S.3.1.3. Multimodal input

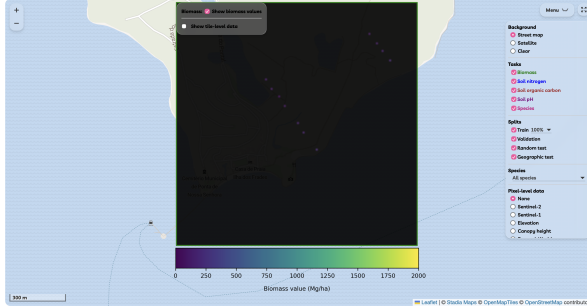
TerraMind is the first any-to-any generative multimodal geospatial model [28]. It is pretrained using a dual token-and pixel-level approach on TerraMesh, a multimodal pre-training dataset with Sentinel-2, Sentinel-1, land use/land cover, NDVI, DEM, geolocation, and captions [9]. We benchmark their TerraMindv1-B model, an architecture based on ViT-B. An extension of DOFA [67], Copernicus-



(a) Full map view.



(b) Zooming in to three biomass tiles and displaying S2.



(c) Displaying biomass pixel-level values.



(d) Tile-level data for the tile.

Figure S.7. **MMEarth-Bench explorer.** Fig. S.7a shows the full map view, where the tiles for all the tasks are overlaid in distinct colors. The user can toggle tasks on and off. Zooming into the map reveals the option to view modality data for the tiles, as shown in Fig. S.7b. The user can click on any of the pixel-level modalities to see the corresponding images overlaid on the tiles in view. Hovering the mouse over a tile reveals the option to see more data, as shown in Fig. S.7c. For biomass, the pixel-level biomass data can be shown. For all the tasks, the user can click to see the values for the tile's tile-level modalities, as shown in Fig. S.7d. Additionally, we will incorporate split data into the map so that users can toggle the tiles by split (train 100%, train 50%, validation, random test, geographic test).

FM is a model that can process data from any spectral or non-spectral sensor with varying resolution through dynamic hypernetworks and also integrates metadata (e.g., geolocation and date) [63]. They pretrain a ViT-B model on the Copernicus-Pretrain dataset [63], which includes data from Sentinel-1, -2, -3, and 5P, as well as Copernicus DEM. As these models mix ascending and descending Sentinel-1 images during training, for each tile we compute the number of valid pixels in the ascending VV and VH bands as well as the number of valid pixels in the descending VV and VH bands. We then take the pair of VV, VH bands that has more valid pixels, either ascending or descending. In the case of a tie we select the ascending VV and VH bands.

### S.3.2. Modality reconstruction

When reconstructing modalities during JT and TTT-MMR, we reconstruct the cyclic-encoded geolocation and month as opposed to the raw values, following prior work [42].

### S.3.3. TTT-MMR-GEO batching

In Fig. S.9 we show an example of the geographically contiguous, non-overlapping batches in TTT-MMR-GEO.

## S.3.4. Evaluation metrics

### S.3.4.1. Coefficient of determination ( $R^2$ )

We use  $R^2$  as the evaluation metric for our regression tasks, where  $R^2 \in (-\infty, 1]$ .

$$R^2 = 1 - \frac{\sum_i (y_i - f(x_i))^2}{\sum_i (y_i - \bar{y})^2}$$

A negative  $R^2$  means that the predictions of the model  $f$  are worse than predicting the mean of the test data  $\bar{y}$ .

### S.3.4.2. Mean Average Precision (mAP)

We use mean average precision as the evaluation metric for our multi-label classification task, where  $\text{mAP} \in [0, 1]$ . This is equivalent to the area under the precision-recall curve.

$$\text{AP} = \sum_n (R_n - R_{n-1}) P_n$$

$P_n$  and  $R_n$  are the precision and recall, respectively, at threshold  $n$ . To calculate mAP, we calculate AP for each class and then compute the mean over all classes.

```
{
  "type": "FeatureCollection",
  "features": [
    {
      "type": "Feature",
      "geometry": {
        "type": "Point",
        "coordinates": [
          lon0,
          lat0
        ]
      },
      "id": 0
    },
    {
      "type": "Feature",
      "geometry": {
        "type": "Point",
        "coordinates": [
          lon1,
          lat1
        ]
      },
      "id": 1
    }
  ]
}
```

Figure S.8. **Example GeoJSON for downloading the MMEarth modalities from (lon, lat) coordinates.** The user should populate the file with the locations where they have downstream task data.

### S.3.4.3. Relative Improvement (RI)

In Tab. 5 we show the average rankings of JT, TTT-MMR, and TTT-MMR-GEO averaged over tasks for each model. Since not all tasks share the same metric, performance deltas cannot simply be averaged across tasks. Moreover, even averaging raw deltas is not ideal for  $R^2$ , as it is nonlinear in the error. One option is to convert changes in  $R^2$  and mAP to a relative improvement metric that can then be averaged across tasks.

$$RI = \frac{\text{metric}_{\text{new}} - \text{metric}_{\text{old}}}{1 - \text{metric}_{\text{old}}}$$

For  $R^2$ , this RI metric can be interpreted as the decrease in the fraction of unexplained variance between two results. For mAP, it represents the decrease in the gap to perfect performance. The fractional relative improvement is multiplied by 100 to yield a relative percent improvement.

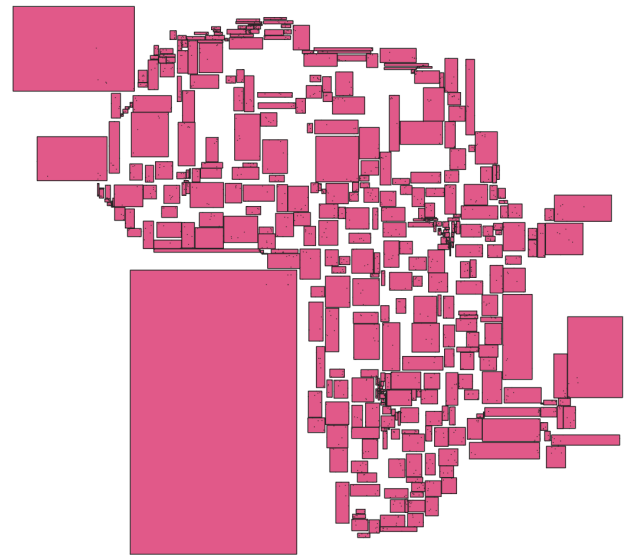


Figure S.9. **Biomass geographic test split batches for TTT-MMR-GEO.** The pink rectangles represent the bounding boxes for the batches. Each black point is a tile in the geographic test set. Each rectangle contains 8 tiles except for one, which contains the batch size (8) plus any remainder (4 in this case).

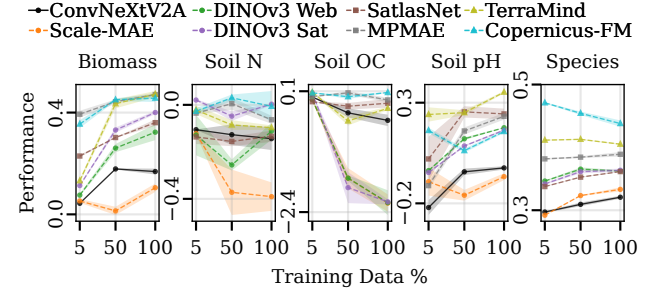


Figure S.10. **Finetuning performance on geographic split.** We observe a weaker relationship between more training data and an improvement in performance than for the random split (Fig. 4).

## S.4. Additional results

### S.4.1. Finetuning vs. linear probing

Fig. S.10 is the equivalent of Fig. 4 but on the geographic test split. Tab. S.9 shows model rankings on each task and overall. We additionally run linear probing experiments, in which the encoder is frozen and only the task decoder is trained. The *linear probing* results are reported in Fig. S.11, Fig. S.12, Fig. S.13, and Fig. S.14, which correspond to the *finetuning* results presented in Fig. 4, Fig. S.10, Fig. 5, and Fig. 6, respectively. For readability, we provide brief interpretations of the results in the figure captions.

Table S.9. **Average model ranks for finetuning on all training data.** Ranks are mean  $\pm$  standard error averaged over seeds, or over tasks and seeds for the “All tasks” column. Lower is better.

Split	Model	Biomass	Soil N	Soil OC	Soil pH	Species	All tasks
Random	ConvNeXtV2A	7.7 $\pm$ 0.3	7.0 $\pm$ 0.0	5.0 $\pm$ 0.0	7.7 $\pm$ 0.3	8.0 $\pm$ 0.0	7.1 $\pm$ 0.3
	Scale-MAE	7.3 $\pm$ 0.3	8.0 $\pm$ 0.0	7.0 $\pm$ 0.6	7.3 $\pm$ 0.3	7.0 $\pm$ 0.0	7.3 $\pm$ 0.2
	DINOv3 Web	5.7 $\pm$ 0.3	4.3 $\pm$ 0.3	6.7 $\pm$ 0.3	4.0 $\pm$ 0.0	6.0 $\pm$ 0.0	5.3 $\pm$ 0.3
	DINOv3 Sat	4.0 $\pm$ 0.0	4.0 $\pm$ 0.6	7.3 $\pm$ 0.7	5.0 $\pm$ 0.0	5.0 $\pm$ 0.0	5.1 $\pm$ 0.4
	SatlasNet	5.3 $\pm$ 0.3	6.0 $\pm$ 0.0	4.0 $\pm$ 0.0	6.0 $\pm$ 0.0	4.0 $\pm$ 0.0	5.1 $\pm$ 0.2
	MPMAE	<b>1.3 <math>\pm</math> 0.3</b>	3.7 $\pm$ 0.7	2.0 $\pm$ 0.0	3.0 $\pm$ 0.0	3.0 $\pm$ 0.0	2.6 $\pm$ 0.3
	TerraMind	2.3 $\pm$ 0.7	<b>1.0 <math>\pm</math> 0.0</b>	3.0 $\pm$ 0.0	<b>1.0 <math>\pm</math> 0.0</b>	2.0 $\pm$ 0.0	1.9 $\pm$ 0.2
	Copernicus-FM	2.3 $\pm$ 0.3	2.0 $\pm$ 0.0	<b>1.0 <math>\pm</math> 0.0</b>	2.0 $\pm$ 0.0	<b>1.0 <math>\pm</math> 0.0</b>	<b>1.7 <math>\pm</math> 0.2</b>
Geographic	ConvNeXtV2A	7.0 $\pm$ 0.0	5.7 $\pm$ 1.3	5.0 $\pm$ 0.0	7.0 $\pm$ 0.0	8.0 $\pm$ 0.0	6.5 $\pm$ 0.4
	Scale-MAE	8.0 $\pm$ 0.0	8.0 $\pm$ 0.0	7.0 $\pm$ 0.6	8.0 $\pm$ 0.0	7.0 $\pm$ 0.0	7.6 $\pm$ 0.2
	DINOv3 Web	5.7 $\pm$ 0.3	4.7 $\pm$ 1.2	6.7 $\pm$ 0.7	4.0 $\pm$ 0.0	5.0 $\pm$ 0.0	5.2 $\pm$ 0.3
	DINOv3 Sat	4.0 $\pm$ 0.0	<b>1.7 <math>\pm</math> 0.3</b>	7.3 $\pm$ 0.3	5.3 $\pm$ 0.3	4.7 $\pm$ 0.7	4.6 $\pm$ 0.5
	SatlasNet	5.3 $\pm$ 0.3	6.0 $\pm$ 0.0	3.0 $\pm$ 0.6	2.3 $\pm$ 0.3	5.3 $\pm$ 0.7	4.4 $\pm$ 0.4
	MPMAE	<b>1.7 <math>\pm</math> 0.3</b>	3.3 $\pm$ 0.7	2.3 $\pm$ 0.3	2.7 $\pm$ 0.3	3.0 $\pm$ 0.0	2.6 $\pm$ 0.2
	TerraMind	2.0 $\pm$ 0.6	4.3 $\pm$ 0.7	3.7 $\pm$ 0.3	<b>1.0 <math>\pm</math> 0.0</b>	2.0 $\pm$ 0.0	2.6 $\pm$ 0.4
	Copernicus-FM	2.3 $\pm$ 0.7	2.3 $\pm$ 1.3	<b>1.0 <math>\pm</math> 0.0</b>	5.7 $\pm$ 0.3	<b>1.0 <math>\pm</math> 0.0</b>	<b>2.5 <math>\pm</math> 0.5</b>

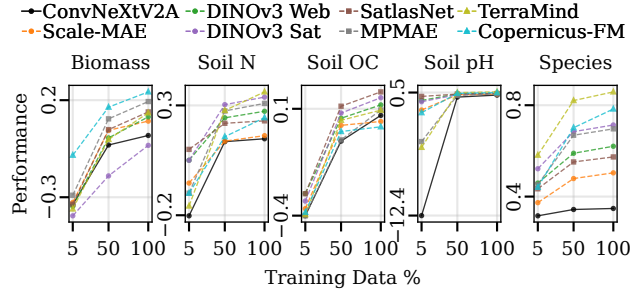


Figure S.11. **Linear probing performance on random split.** As for finetuning in Fig. 4., performance improves with more training data on the random split.

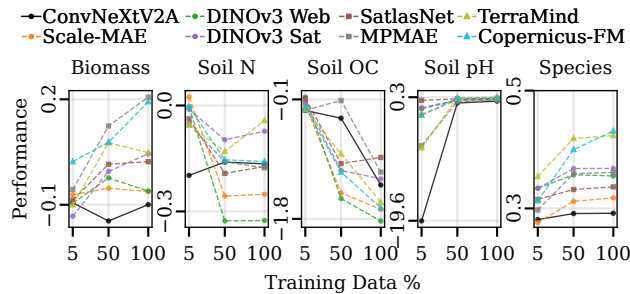


Figure S.12. **Linear probing performance on geographic split.** As in Fig. S.10, more training data usually improves performance on the geographic split but not always. Soil OC is a consistent counterexample.

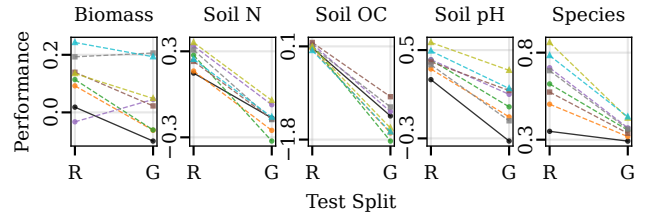


Figure S.13. **Geographic generalization for linear probing.** Performance comparison on random (R) vs. geographic (G) test splits using all training data. As in Fig. 5 for finetuning, all the tasks other than biomass suffer large performance drops when switching from the random to the geographic test split. We generally see a less severe geographic generalization gap for linear probing than finetuning. This could be due to linear probing having a lower capacity for fitting to the source domain than finetuning.

#### S.4.2. Test-time training performance with relative improvement metric

Fig. S.15 is analogous to Fig. 7 except using the relative improvement metric instead of the raw delta.

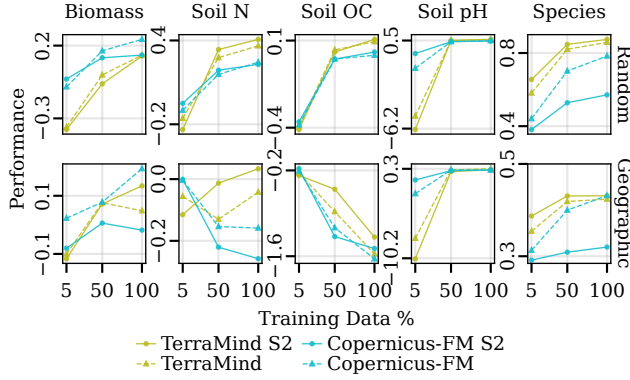


Figure S.14. **Unimodal vs. multimodal input data for linear probing.** We see similar patterns as for finetuning in Fig. 6.

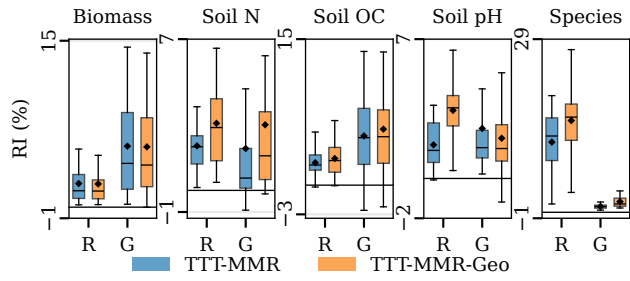


Figure S.15. **Multimodal test-time training relative improvement (RI) per task.** RI represents the relative improvement ( $\frac{\text{TTT}-\text{JT}}{1-\text{JT}}$ ) (multiplied by 100 to express a percentage). Patterns are generally consistent with Fig. 7, which showed the raw deltas. With the RI metric, however, we see that TTT leads to the greatest performance gains on the random split for species rather than the geographic split of soil OC, where  $R^2$  values are mostly negative before and after TTT.

#### S.4.3. Modality reconstruction visualization

Fig. S.16 compares the original pixel-level modalities to their reconstructed forms following JT and TTT-MMR. In particular, we visualize a batch of tiles in the soil nitrogen random test set when run with the MPMAE pretrained model.

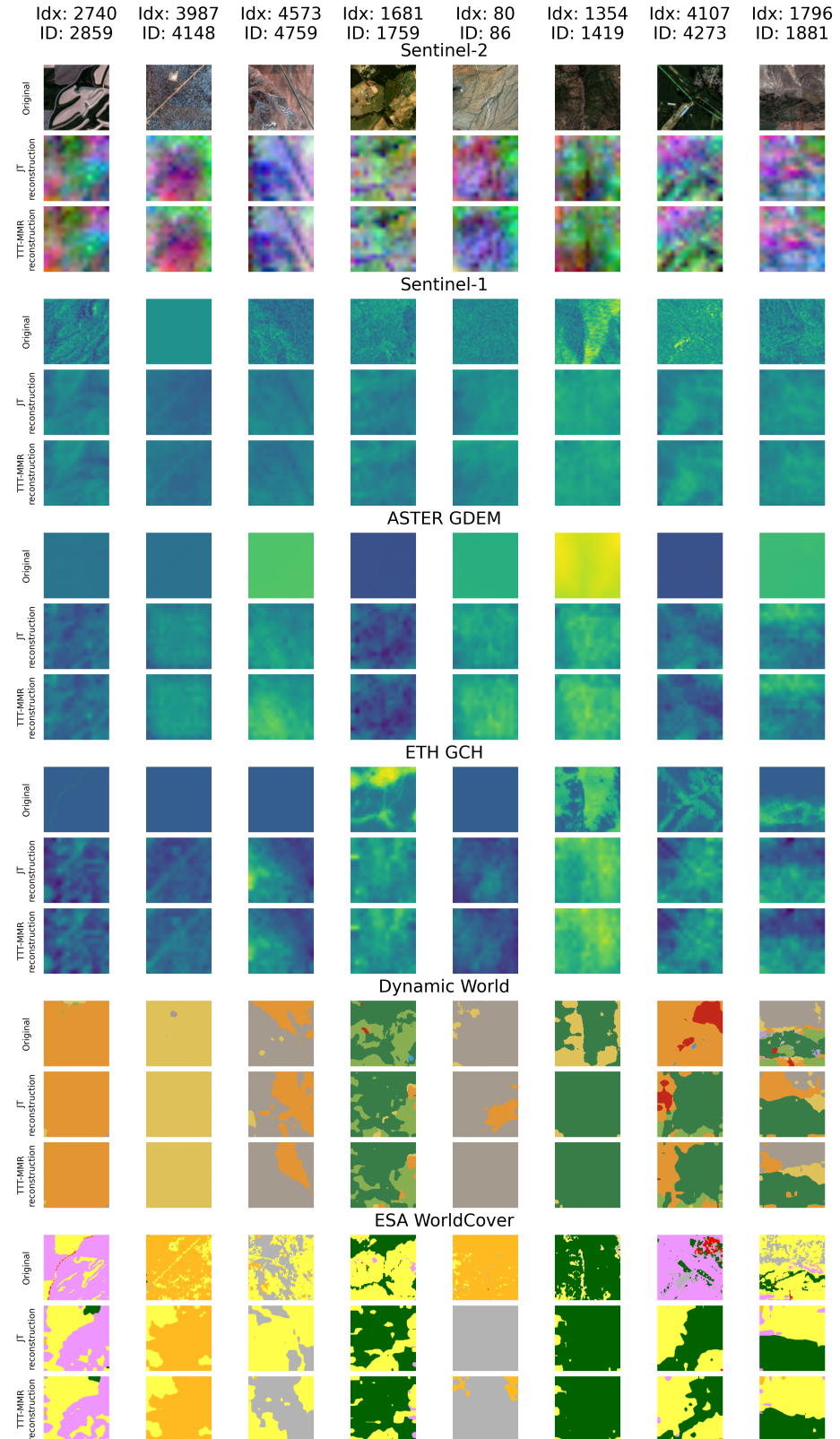


Figure S.16. **Pixel-level modality reconstructions.** MPMAE reconstructions after JT and TTT-MMR as compared to the original. Tiles are from the soil nitrogen random test set.

Table S.10. **Multimodal test-time training relative improvement (RI) per model.** Average improvement over JT of TTT-MMR and TTT-MMR-GEO. Values show the relative improvement ( $\frac{\text{TTT} - \text{JT}}{1 - \text{JT}}$ ) as mean  $\pm$  standard error (multiplied by 100 to represent a percentage) averaged over tasks and seeds. Higher is better. Whereas in Tab. 5 which compared method rankings TTT-MMR was the best method for SatlasNet on the geographic split, according to the RI metric TTT-MMR-GEO is the best method for all models and splits. These RI values support the claim in the main paper that the RGB-only models tend to undergo larger performance improvements as a result of TTT than the multimodal models. MPMAE benefits less from TTT than the RGB-only models and SatlasNet but more than the multimodal models.

Split	Method	ConvNeXtV2A	Scale-MAE	DINOv3 Web	DINOv3 Sat	SatlasNet	MPMAE	TerraMind	Copernicus-FM
<b>Random</b>	TTT-MMR	$3.5 \pm 0.7$	$5.2 \pm 1.4$	$5.5 \pm 1.6$	$5.0 \pm 1.2$	$5.7 \pm 1.9$	$3.9 \pm 1.1$	$2.7 \pm 1.0$	$0.4 \pm 0.1$
	TTT-MMR-Geo	<b><math>8.1 \pm 1.1</math></b>	<b><math>5.9 \pm 1.6</math></b>	<b><math>6.2 \pm 1.9</math></b>	<b><math>5.6 \pm 1.4</math></b>	<b><math>9.0 \pm 2.8</math></b>	<b><math>4.3 \pm 1.0</math></b>	<b><math>3.1 \pm 1.2</math></b>	<b><math>0.5 \pm 0.2</math></b>
<b>Geographic</b>	TTT-MMR	$9.0 \pm 1.3$	$2.7 \pm 0.7$	$3.5 \pm 0.7$	$3.4 \pm 1.1$	$3.9 \pm 2.0$	$1.8 \pm 0.6$	$0.8 \pm 0.3$	$0.6 \pm 0.1$
	TTT-MMR-Geo	<b><math>9.1 \pm 1.4</math></b>	<b><math>2.9 \pm 0.7</math></b>	<b><math>3.6 \pm 0.6</math></b>	<b><math>3.6 \pm 1.2</math></b>	<b><math>5.1 \pm 1.9</math></b>	<b><math>2.7 \pm 0.7</math></b>	<b><math>1.0 \pm 0.3</math></b>	<b><math>0.9 \pm 0.2</math></b>

## S.5. Raw results

For completeness, we provide the raw numbers underlying all the results figures in the main paper and supplementary. We bold the result for the best model (vertical comparison).

### S.5.1. Finetuning

The “Random” section of Tabs. S.11 to S.15 shows the numbers used to create Fig. 4. The “100%” columns in Tabs. S.11 to S.15 were used to generate Fig. 5. We made Fig. 6. based off the “TerraMindS2”, “TerraMind”, “Copernicus-FMS2”, and “Copernicus-FM” rows in Tabs. S.11 to S.15. The “Geographic” section of Tabs. S.11 to S.15 shows the numbers used to create Fig. S.10.

Table S.11. Biomass finetuning test  $R^2$ 

	Random									Geographic									
	Seed 41			Seed 42			Seed 43			Seed 41			Seed 42			Seed 43			
	5%	50%	100%		5%	50%	100%		5%	50%	100%		5%	50%	100%		5%	50%	100%
ConvNeXtV2A	-0.15	0.13	0.16	-0.15	0.13	0.16	-0.15	0.13	0.15	0.04	0.18	0.16	0.05	0.18	0.19	0.04	0.17	0.15	
Scale-MAE	0.03	0.13	0.16	0.02	0.13	0.16	0.01	0.12	0.17	0.06	-0.01	0.13	0.04	0.05	0.10	0.06	0.00	0.08	
DINOv3 Web	0.01	0.32	0.38	0.01	0.31	0.38	0.01	0.32	0.38	0.07	0.29	0.26	0.08	0.23	0.35	0.08	0.26	0.36	
DINOv3 Sat	0.02	0.33	0.40	0.00	0.34	0.39	0.01	0.35	0.40	0.11	0.33	0.39	0.11	0.32	0.41	0.12	0.35	0.40	
SatlasNet	0.22	0.36	0.39	0.21	0.35	0.38	0.22	0.35	0.38	0.22	0.30	0.37	0.24	0.30	0.37	0.23	0.30	0.34	
MPMAE	<b>0.36</b>	0.42	<b>0.45</b>	<b>0.36</b>	0.40	<b>0.45</b>	<b>0.36</b>	0.41	<b>0.45</b>	<b>0.37</b>	<b>0.46</b>	<b>0.48</b>	<b>0.42</b>	0.43	0.47	<b>0.39</b>	0.45	0.46	
TerraMind S2	-0.04	0.34	0.41	-0.03	0.35	0.42	-0.03	0.35	0.41	0.12	0.42	0.44	0.14	0.37	0.46	0.13	0.40	0.44	
TerraMind	-0.05	0.34	0.43	-0.04	0.37	<b>0.45</b>	-0.04	0.39	0.42	0.12	0.40	<b>0.48</b>	0.14	<b>0.44</b>	<b>0.49</b>	0.14	<b>0.46</b>	0.45	
Copernicus-FM S2	0.21	0.37	0.41	0.19	0.36	0.41	0.21	0.37	0.41	0.28	0.35	0.40	0.24	0.40	0.38	0.28	0.39	0.43	
Copernicus-FM	0.34	<b>0.44</b>	0.44	0.33	<b>0.43</b>	0.44	0.34	<b>0.43</b>	0.44	0.36	0.45	0.43	0.38	<b>0.44</b>	0.45	0.33	<b>0.46</b>	<b>0.49</b>	

Table S.12. Soil nitrogen finetuning test  $R^2$ 

	Random									Geographic									
	Seed 41			Seed 42			Seed 43			Seed 41			Seed 42			Seed 43			
	5%	50%	100%		5%	50%	100%		5%	50%	100%		5%	50%	100%		5%	50%	100%
ConvNeXtV2A	0.18	0.22	0.22	0.18	0.20	0.20	0.18	0.21	0.22	-0.11	-0.19	-0.07	-0.11	-0.15	-0.12	-0.10	-0.04	-0.24	
Scale-MAE	0.10	0.18	0.16	0.08	0.19	0.19	0.10	0.17	0.20	-0.12	-0.19	-0.49	-0.13	-0.40	-0.40	-0.11	-0.52	-0.28	
DINOv3 Web	0.14	0.34	0.39	0.18	0.35	0.36	0.19	0.33	0.38	-0.07	-0.22	-0.17	-0.30	-0.25	-0.05	-0.02	-0.30	-0.12	
DINOv3 Sat	0.23	0.34	0.37	0.21	0.34	0.38	0.22	0.33	0.38	<b>0.01</b>	-0.09	0.01	<b>0.03</b>	-0.02	0.00	<b>0.02</b>	-0.04	<b>-0.00</b>	
SatlasNet	0.17	0.25	0.31	0.19	0.30	0.31	0.18	0.27	0.32	-0.19	-0.18	-0.10	-0.12	-0.12	-0.12	-0.09	-0.17	-0.18	
MPMAE	0.29	0.40	0.42	0.30	0.41	<b>0.45</b>	0.29	0.41	0.38	-0.05	-0.04	-0.08	-0.03	<b>0.05</b>	-0.08	-0.03	0.01	-0.03	
TerraMind S2	<b>0.40</b>	0.43	0.48	0.36	<b>0.46</b>	0.47	0.37	0.42	<b>0.50</b>	-0.04	-0.02	0.01	-0.06	-0.01	-0.04	-0.04	-0.08	-0.04	
TerraMind	0.33	<b>0.46</b>	<b>0.50</b>	0.37	0.44	<b>0.51</b>	0.37	<b>0.48</b>	<b>0.50</b>	-0.03	-0.10	-0.08	-0.05	-0.05	-0.11	0.01	-0.11	-0.09	
Copernicus-FM S2	0.25	0.34	0.31	0.25	0.33	0.34	0.25	0.34	0.35	-0.09	-0.05	-0.08	-0.13	-0.02	-0.11	-0.11	-0.18	-0.09	
Copernicus-FM	0.38	0.44	0.44	<b>0.39</b>	<b>0.46</b>	0.46	<b>0.39</b>	0.46	0.48	-0.05	<b>0.02</b>	<b>0.04</b>	-0.02	0.01	<b>0.08</b>	-0.01	<b>0.06</b>	-0.13	

Table S.13. Soil organic carbon finetuning test  $R^2$ 

	Random									Geographic									
	Seed 41			Seed 42			Seed 43			Seed 41			Seed 42			Seed 43			
	5%	50%	100%		5%	50%	100%		5%	50%	100%		5%	50%	100%		5%	50%	100%
ConvNeXtV2A	-0.26	0.14	0.21	-0.26	0.14	0.18	-0.26	0.14	0.19	-0.01	-0.50	-0.72	-0.02	-0.37	-0.31	-0.02	-0.17	-0.48	
Scale-MAE	<b>-0.09</b>	0.09	0.13	<b>-0.09</b>	0.06	0.10	<b>-0.10</b>	0.09	0.10	-0.05	-1.55	-2.21	-0.13	-2.11	-1.90	-0.04	-1.43	-2.52	
DINOv3 Web	-0.10	0.10	0.11	<b>-0.09</b>	0.08	0.12	<b>-0.09</b>	0.09	0.10	0.02	-1.74	-1.92	-0.12	-1.58	-2.72	-0.12	-1.77	-1.97	
DINOv3 Sat	-0.10	0.08	0.05	-0.10	0.09	0.08	-0.11	0.06	0.12	0.08	-2.54	-2.22	0.05	-1.56	-2.08	<b>0.07</b>	-1.58	-2.26	
SatlasNet	-0.10	0.18	0.30	-0.10	0.30	0.31	-0.10	0.28	0.31	-0.12	-0.32	-0.03	-0.12	-0.09	-0.09	-0.12	-0.21	-0.32	
MPMAE	-0.26	0.22	0.40	-0.26	0.23	0.40	-0.26	0.24	0.40	-0.01	<b>0.04</b>	0.01	-0.01	<b>0.14</b>	-0.12	-0.01	0.02	-0.13	
TerraMind S2	-0.13	0.34	0.31	-0.14	0.31	0.31	-0.14	0.33	0.28	0.06	-0.01	0.04	0.06	-0.03	0.02	<b>0.07</b>	<b>0.04</b>	0.02	
TerraMind	-0.14	0.30	0.33	-0.14	0.34	0.34	-0.15	0.33	0.33	<b>0.10</b>	-0.68	-0.20	<b>0.07</b>	-0.35	-0.25	<b>0.07</b>	-0.52	-0.32	
Copernicus-FM S2	-0.15	0.28	0.30	-0.15	0.25	0.31	-0.14	0.31	0.27	0.05	-0.30	-0.23	<b>0.07</b>	-0.00	-0.05	0.06	-0.06	-0.10	
Copernicus-FM	-0.14	<b>0.41</b>	<b>0.45</b>	-0.14	<b>0.44</b>	<b>0.50</b>	-0.14	<b>0.39</b>	<b>0.47</b>	0.07	-0.10	<b>0.09</b>	0.06	0.04	<b>0.08</b>	<b>0.07</b>	0.02	<b>0.05</b>	

Table S.14. Soil pH finetuning test  $R^2$ 

	Random									Geographic									
	Seed 41			Seed 42			Seed 43			Seed 41			Seed 42			Seed 43			
	5%	50%	100%		5%	50%	100%		5%	50%	100%		5%	50%	100%		5%	50%	100%
ConvNeXtV2A	0.37	0.38	0.39	0.37	0.38	0.42	0.37	0.39	0.37	-0.29	-0.08	-0.03	-0.16	-0.03	-0.01	-0.22	-0.03	-0.04	
Scale-MAE	0.28	0.37	0.40	0.29	0.38	0.39	0.29	0.36	0.39	-0.23	-0.21	-0.07	-0.02	-0.12	-0.04	-0.03	-0.15	-0.10	
DINOv3 Web	0.40	0.51	0.56	0.41	0.50	0.55	0.41	0.50	0.55	-0.03	0.13	0.18	-0.04	0.13	0.18	-0.05	0.11	0.18	
DINOv3 Sat	0.38	0.49	0.54	0.37	0.49	0.55	0.38	0.50	0.54	-0.04	0.08	0.16	-0.06	0.09	0.17	-0.04	0.09	0.16	
SatlasNet	0.40	0.47	0.52	0.41	0.45	0.50	0.42	0.48	0.50	-0.20	0.22	0.29	0.14	0.24	0.20	0.12	<b>0.31</b>	0.23	
MPMAE	0.40	0.55	0.57	0.41	0.53	0.56	0.39	0.54	0.58	-0.15	0.16	0.21	-0.08	0.13	0.27	-0.11	0.19	0.22	
TerraMind S2	0.50	0.61	0.66	0.50	0.61	0.65	0.48	0.61	0.64	0.22	0.22	0.35	<b>0.27</b>	<b>0.26</b>	0.32	0.05	0.25	0.32	
TerraMind	<b>0.52</b>	<b>0.62</b>	<b>0.67</b>	<b>0.51</b>	<b>0.62</b>	<b>0.67</b>	<b>0.51</b>	<b>0.63</b>	<b>0.67</b>	<b>0.24</b>	<b>0.24</b>	<b>0.36</b>	0.18	0.23	<b>0.36</b>	<b>0.30</b>	0.27	<b>0.34</b>	
Copernicus-FM S2	0.46	0.51	0.55	0.46	0.50	0.56	0.47	0.50	0.55	0.10	0.17	0.26	0.11	0.17	0.26	0.11	0.14	0.26	
Copernicus-FM	0.5																		

Table S.15. Species finetuning test mAP

	Random									Geographic								
	Seed 41			Seed 42			Seed 43			Seed 41			Seed 42			Seed 43		
	5%	50%	100%	5%	50%	100%	5%	50%	100%	5%	50%	100%	5%	50%	100%	5%	50%	100%
ConvNeXtV2A	0.37	0.45	0.47	0.37	0.43	0.48	0.38	0.45	0.48	0.30	0.31	0.32	0.30	0.31	0.32	0.30	0.30	0.32
Scale-MAE	0.43	0.61	0.67	0.43	0.60	0.67	0.44	0.61	0.67	0.29	0.32	0.33	0.29	0.32	0.33	0.29	0.32	0.34
DINOv3 Web	0.56	0.77	0.82	0.56	0.76	0.82	0.56	0.77	0.82	0.34	0.37	0.36	0.35	0.37	0.36	0.35	0.36	0.36
DINOv3 Sat	0.58	0.77	0.82	0.58	0.77	0.83	0.58	0.78	0.83	0.34	0.36	0.36	0.34	0.36	0.37	0.34	0.36	0.36
SatlasNet	0.61	0.78	0.84	0.62	0.79	0.84	0.62	0.78	0.84	0.34	0.35	0.36	0.34	0.35	0.36	0.34	0.35	0.36
MPMAE	0.70	0.87	0.90	0.71	0.87	0.90	0.70	0.87	0.90	0.38	0.38	0.39	0.38	0.39	0.39	0.38	0.38	0.38
TerraMind S2	0.80	0.91	0.93	0.80	0.91	0.93	0.80	0.91	0.93	0.41	0.42	0.41	0.41	0.41	0.41	0.41	0.42	0.41
TerraMind	0.83	0.93	0.95	0.83	0.93	0.95	0.82	0.93	0.95	0.41	0.41	0.41	0.41	0.41	0.41	0.41	0.41	0.40
Copernicus-FM S2	0.65	0.83	0.88	0.66	0.84	0.88	0.66	0.84	0.87	0.34	0.38	0.37	0.34	0.37	0.38	0.34	0.37	0.39
Copernicus-FM	<b>0.92</b>	<b>0.99</b>	<b>0.99</b>	<b>0.91</b>	<b>0.99</b>	<b>0.99</b>	<b>0.91</b>	<b>0.99</b>	<b>0.99</b>	<b>0.47</b>	<b>0.46</b>	<b>0.45</b>	<b>0.47</b>	<b>0.45</b>	<b>0.43</b>	<b>0.47</b>	<b>0.45</b>	<b>0.44</b>

### S.5.2. Joint training and test-time training

The “JT”, “TTT-MMR”, and “TTT-MMR-Geo” columns in Tabs. S.16 to S.30 were used to create Fig. 7. We additionally underline the result for the best method (horizontal comparison).

Model	Random				Geographic			
	FT	JT	TTT-MMR	TTT-MMR-Geo	FT	JT	TTT-MMR	TTT-MMR-Geo
ConvNeXtV2A	0.15	0.16	0.19	<u>0.20</u>	0.15	0.12	0.23	<u>0.24</u>
Scale-MAE	0.17	0.18	<u>0.19</u>	0.19	0.08	0.11	<u>0.14</u>	0.14
DINOv3 Web	<u>0.38</u>	0.37	<u>0.38</u>	<u>0.38</u>	<u>0.36</u>	0.32	<u>0.36</u>	0.35
DINOv3 Sat	<u>0.40</u>	0.39	0.39	0.39	<u>0.40</u>	0.37	0.39	0.39
SatlasNet	0.38	0.39	<u>0.41</u>	<u>0.41</u>	0.34	0.37	<u>0.44</u>	0.43
MPMAE	<b>0.45</b>	<b>0.46</b>	<u>0.47</u>	<u>0.46</u>	0.46	0.48	<u>0.48</u>	<u>0.48</u>
TerraMind	0.42	0.44	<u>0.45</u>	<u>0.45</u>	0.45	<u>0.51</u>	<u>0.51</u>	<u>0.51</u>
Copernicus-FM	<u>0.44</u>	0.43	<u>0.44</u>	<u>0.44</u>	<u>0.49</u>	0.47	0.48	0.48

Table S.18. Biomass test  $R^2$  by architecture, adaptation mode, and split (Seed 43)

Model	Random				Geographic			
	FT	JT	TTT-MMR	TTT-MMR-Geo	FT	JT	TTT-MMR	TTT-MMR-Geo
ConvNeXtV2A	0.22	0.22	0.24	<u>0.26</u>	-0.07	-0.07	<u>-0.01</u>	-0.02
Scale-MAE	0.16	0.18	<u>0.20</u>	<u>0.20</u>	-0.49	<u>-0.42</u>	<u>-0.42</u>	-0.42
DINOv3 Web	0.39	0.38	0.40	<u>0.41</u>	-0.17	-0.23	<u>-0.16</u>	-0.16
DINOv3 Sat	0.37	0.37	0.38	<u>0.39</u>	0.01	-0.03	-0.02	-0.02
SatlasNet	0.31	0.30	0.33	<u>0.35</u>	-0.10	-0.09	-0.10	-0.04
MPMAE	0.42	0.44	<u>0.45</u>	<u>0.45</u>	-0.08	<u>-0.02</u>	-0.04	-0.03
TerraMind	<b>0.50</b>	<b>0.49</b>	<b>0.49</b>	<b>0.49</b>	-0.08	-0.16	-0.16	-0.15
Copernicus-FM	0.44	0.46	0.46	0.46	<u>0.04</u>	<u>0.05</u>	<u>0.05</u>	<u>0.05</u>

Table S.19. Soil nitrogen test  $R^2$  by architecture, adaptation mode, and split (Seed 41)

Model	Random				Geographic			
	FT	JT	TTT-MMR	TTT-MMR-Geo	FT	JT	TTT-MMR	TTT-MMR-Geo
ConvNeXtV2A	0.20	0.20	0.22	<u>0.23</u>	-0.12	-0.12	<u>-0.07</u>	-0.07
Scale-MAE	<u>0.19</u>	0.17	<u>0.19</u>	<u>0.19</u>	-0.40	-0.50	-0.50	-0.49
DINOv3 Web	0.36	0.38	<u>0.39</u>	<u>0.39</u>	-0.05	-0.04	-0.03	-0.02
DINOv3 Sat	0.38	0.38	0.38	<u>0.39</u>	0.00	<b>0.01</b>	<b>0.01</b>	0.02
SatlasNet	0.31	0.30	0.36	<u>0.37</u>	-0.12	-0.23	-0.06	<b>0.05</b>
MPMAE	0.45	0.41	0.43	0.43	-0.08	-0.03	-0.02	-0.01
TerraMind	<b>0.51</b>	<b>0.51</b>	<b>0.51</b>	<b>0.51</b>	-0.11	-0.12	-0.12	-0.12
Copernicus-FM	0.46	0.48	0.48	0.49	<u>0.08</u>	-0.05	-0.04	-0.02

Table S.20. Soil nitrogen test  $R^2$  by architecture, adaptation mode, and split (Seed 42)

Model	Random				Geographic			
	FT	JT	TTT-MMR	TTT-MMR-Geo	FT	JT	TTT-MMR	TTT-MMR-Geo
ConvNeXtV2A	0.22	0.22	0.24	<u>0.27</u>	-0.24	-0.19	<u>-0.08</u>	-0.09
Scale-MAE	<u>0.20</u>	0.15	0.17	0.18	<u>0.28</u>	-0.31	-0.30	-0.29
DINOv3 Web	0.38	0.39	<u>0.40</u>	<u>0.40</u>	-0.12	-0.09	<u>-0.07</u>	-0.07
DINOv3 Sat	0.38	0.39	0.41	<u>0.42</u>	<b>-0.00</b>	-0.03	-0.02	-0.02
SatlasNet	0.32	0.31	0.32	<u>0.35</u>	-0.18	-0.08	-0.07	-0.01
MPMAE	0.38	0.40	0.42	0.42	-0.03	-0.05	-0.05	-0.05
TerraMind	<b>0.50</b>	<b>0.49</b>	<b>0.50</b>	<b>0.50</b>	-0.09	-0.08	<u>-0.07</u>	-0.07
Copernicus-FM	0.48	0.46	0.46	0.46	-0.13	<b>0.04</b>	<b>0.04</b>	<b>0.04</b>

Table S.21. Soil nitrogen test  $R^2$  by architecture, adaptation mode, and split (Seed 43)

Model	Random				Geographic			
	FT	JT	TTT-MMR	TTT-MMR-Geo	FT	JT	TTT-MMR	TTT-MMR-Geo
ConvNeXtV2A	0.21	0.22	0.24	<u>0.25</u>	-0.72	-0.62	<u>-0.45</u>	-0.50
Scale-MAE	<u>0.13</u>	0.09	0.11	0.11	<u>-2.21</u>	-3.20	-3.07	-3.04
DINOv3 Web	0.11	0.12	<u>0.15</u>	<u>0.15</u>	<u>-1.92</u>	-2.07	-1.95	<u>-1.92</u>
DINOv3 Sat	0.05	0.10	0.15	<u>0.16</u>	<u>-2.22</u>	-2.07	-1.61	<u>-1.52</u>
SatlasNet	0.30	0.33	0.31	<u>0.33</u>	<u>-0.03</u>	-0.08	-0.25	-0.17
MPMAE	0.40	0.38	0.39	<u>0.40</u>	0.01	0.00	<u>0.01</u>	0.01
TerraMind	0.33	0.32	<u>0.33</u>	<u>0.33</u>	-0.20	-0.11	-0.09	-0.08
Copernicus-FM	<b>0.45</b>	<b>0.45</b>	<b>0.45</b>	<b>0.45</b>	<b>0.09</b>	<b>0.03</b>	<b>0.03</b>	<b>0.03</b>

Table S.22. Soil organic carbon test  $R^2$  by architecture, adaptation mode, and split (Seed 41)

Model	Random				Geographic			
	FT	JT	TTT-MMR	TTT-MMR-Geo	FT	JT	TTT-MMR	TTT-MMR-Geo
ConvNeXtV2A	0.18	0.18	<u>0.25</u>	<u>0.25</u>	-0.31	-0.42	<u>-0.18</u>	-0.22
Scale-MAE	0.10	0.10	<u>0.11</u>	<u>0.11</u>	<u>-1.90</u>	-2.13	<u>-2.02</u>	-2.00
DINOv3 Web	0.12	0.12	<u>0.17</u>	<u>0.17</u>	<u>-2.72</u>	-3.22	-2.80	-2.81
DINOv3 Sat	0.08	0.11	<u>0.14</u>	<u>0.14</u>	-0.08	-1.88	<u>-1.55</u>	-1.56
SatlasNet	0.31	0.32	<u>0.34</u>	<u>0.34</u>	<u>-0.09</u>	-0.40	-0.21	-0.25
MPMAE	0.40	0.40	<u>0.41</u>	<u>0.41</u>	-0.12	-0.00	0.04	<u>0.05</u>
TerraMind	0.34	0.34	<u>0.36</u>	<u>0.36</u>	-0.25	-0.46	-0.41	-0.40
Copernicus-FM	<b>0.50</b>	<b>0.46</b>	<b>0.46</b>	<b>0.46</b>	<b>0.08</b>	<b>0.06</b>	<b>0.06</b>	<b>0.06</b>

Table S.23. Soil organic carbon test  $R^2$  by architecture, adaptation mode, and split (Seed 42)

Model	Random				Geographic			
	FT	JT	TTT-MMR	TTT-MMR-Geo	FT	JT	TTT-MMR	TTT-MMR-Geo
ConvNeXtV2A	0.19	0.20	0.22	<b>0.24</b>	-0.48	-0.75	-0.55	<b>-0.38</b>
Scale-MAE	<b>0.10</b>	0.08	0.09	<b>0.10</b>	-2.52	-1.60	-1.56	<b>-1.53</b>
DINOv3 Web	0.10	0.13	<b>0.16</b>	<b>0.16</b>	-1.97	-2.02	-1.85	<b>-1.82</b>
DINOv3 Sat	0.12	0.09	<b>0.14</b>	<b>0.13</b>	-2.26	-2.19	<b>-2.05</b>	-2.06
SatlasNet	0.31	0.31	0.32	<b>0.34</b>	-0.32	-0.25	<b>-0.19</b>	-0.22
MPMAE	0.40	0.40	<b>0.41</b>	<b>0.41</b>	-0.13	<b>0.08</b>	<b>0.15</b>	<b>0.17</b>
TerraMind	0.33	0.34	<b>0.35</b>	<b>0.35</b>	<b>-0.32</b>	-1.06	-0.99	-0.98
Copernicus-FM	<b>0.47</b>	<b>0.47</b>	<b>0.46</b>	<b>0.46</b>	<b>0.05</b>	<b>0.08</b>	<b>0.08</b>	<b>0.08</b>

Table S.24. Soil organic carbon test  $R^2$  by architecture, adaptation mode, and split (Seed 43)

Model	Random				Geographic			
	FT	JT	TTT-MMR	TTT-MMR-Geo	FT	JT	TTT-MMR	TTT-MMR-Geo
ConvNeXtV2A	0.39	0.41	0.42	<b>0.46</b>	-0.03	0.04	<b>0.14</b>	0.13
Scale-MAE	0.40	0.43	0.45	<b>0.46</b>	-0.07	-0.01	<b>0.01</b>	0.01
DINOv3 Web	0.56	0.58	<b>0.59</b>	<b>0.59</b>	0.18	0.23	<b>0.25</b>	0.25
DINOv3 Sat	0.54	0.56	<b>0.58</b>	<b>0.58</b>	0.16	0.20	<b>0.21</b>	<b>0.21</b>
SatlasNet	0.52	0.54	0.54	<b>0.56</b>	<b>0.29</b>	0.20	0.21	0.19
MPMAE	0.57	0.59	0.59	<b>0.60</b>	0.21	0.26	0.27	<b>0.29</b>
TerraMind	<b>0.67</b>	<b>0.67</b>	<b>0.68</b>	<b>0.68</b>	<b>0.36</b>	<b>0.35</b>	<b>0.35</b>	<b>0.35</b>
Copernicus-FM	0.63	<b>0.65</b>	<b>0.65</b>	<b>0.65</b>	0.17	0.19	0.19	<b>0.20</b>

Table S.25. Soil pH test  $R^2$  by architecture, adaptation mode, and split (Seed 41)

Model	Random				Geographic			
	FT	JT	TTT-MMR	TTT-MMR-Geo	FT	JT	TTT-MMR	TTT-MMR-Geo
ConvNeXtV2A	0.42	0.42	0.41	<b>0.46</b>	-0.01	0.05	<b>0.16</b>	0.12
Scale-MAE	0.39	0.42	0.44	<b>0.45</b>	-0.04	-0.00	0.02	<b>0.03</b>
DINOv3 Web	0.55	0.58	<b>0.59</b>	<b>0.59</b>	0.18	0.26	<b>0.27</b>	<b>0.27</b>
DINOv3 Sat	0.55	0.57	<b>0.58</b>	<b>0.58</b>	0.17	0.22	<b>0.23</b>	0.23
SatlasNet	0.50	0.55	0.55	<b>0.56</b>	0.20	0.20	<b>0.22</b>	0.22
MPMAE	0.56	0.59	0.60	<b>0.61</b>	0.27	0.26	<b>0.28</b>	0.27
TerraMind	<b>0.67</b>	<b>0.67</b>	<b>0.68</b>	<b>0.68</b>	<b>0.36</b>	<b>0.35</b>	<b>0.35</b>	<b>0.35</b>
Copernicus-FM	0.62	<b>0.65</b>	<b>0.65</b>	<b>0.65</b>	0.15	0.19	<b>0.20</b>	<b>0.20</b>

Table S.26. Soil pH test  $R^2$  by architecture, adaptation mode, and split (Seed 42)

Model	Random				Geographic			
	FT	JT	TTT-MMR	TTT-MMR-Geo	FT	JT	TTT-MMR	TTT-MMR-Geo
ConvNeXtV2A	0.37	0.40	0.40	<b>0.44</b>	-0.04	0.03	<b>0.10</b>	0.08
Scale-MAE	0.39	0.43	0.45	<b>0.46</b>	-0.04	-0.03	<b>0.02</b>	<b>0.03</b>
DINOv3 Web	0.55	0.58	<b>0.59</b>	<b>0.59</b>	0.18	0.26	<b>0.27</b>	<b>0.27</b>
DINOv3 Sat	0.55	0.57	<b>0.58</b>	<b>0.58</b>	0.17	0.22	<b>0.23</b>	0.23
SatlasNet	0.50	0.54	0.55	<b>0.56</b>	0.23	0.22	<b>0.23</b>	0.20
MPMAE	0.58	0.59	0.60	<b>0.61</b>	0.22	0.21	0.23	<b>0.24</b>
TerraMind	<b>0.67</b>	<b>0.67</b>	<b>0.68</b>	<b>0.68</b>	<b>0.34</b>	<b>0.33</b>	<b>0.33</b>	<b>0.33</b>
Copernicus-FM	0.62	<b>0.65</b>	<b>0.65</b>	<b>0.65</b>	0.15	0.20	<b>0.20</b>	<b>0.20</b>

Table S.27. Soil pH test  $R^2$  by architecture, adaptation mode, and split (Seed 43)

Model	Random				Geographic			
	FT	JT	TTT-MMR	TTT-MMR-Geo	FT	JT	TTT-MMR	TTT-MMR-Geo
ConvNeXtV2A	0.47	0.53	0.55	<b>0.60</b>	0.32	0.32	0.33	<b>0.34</b>
Scale-MAE	0.67	0.72	0.76	<b>0.77</b>	0.33	0.33	<b>0.34</b>	<b>0.34</b>
DINOv3 Web	0.82	0.84	<b>0.87</b>	<b>0.87</b>	0.36	0.36	<b>0.37</b>	<b>0.37</b>
DINOv3 Sat	0.82	0.84	<b>0.86</b>	<b>0.86</b>	0.36	0.36	<b>0.37</b>	<b>0.37</b>
SatlasNet	0.84	0.86	0.89	<b>0.90</b>	0.36	0.38	0.38	0.39
MPMAE	0.90	0.90	<b>0.92</b>	0.91	0.39	0.40	<b>0.41</b>	<b>0.41</b>
TerraMind	<b>0.95</b>	<b>0.95</b>	<b>0.95</b>	<b>0.95</b>	<b>0.41</b>	<b>0.40</b>	<b>0.41</b>	<b>0.41</b>
Copernicus-FM	<b>0.99</b>	<b>0.99</b>	<b>0.99</b>	<b>0.99</b>	<b>0.45</b>	<b>0.47</b>	<b>0.47</b>	<b>0.48</b>

Table S.28. Species test mAP by architecture, adaptation mode, and split (Seed 41)

Model	Random				Geographic			
	FT	JT	TTT-MMR	TTT-MMR-Geo	FT	JT	TTT-MMR	TTT-MMR-Geo
ConvNeXtV2A	0.48	0.53	0.55	<b>0.59</b>	0.32	0.33	0.34	<b>0.35</b>
Scale-MAE	0.67	0.72	0.76	<b>0.77</b>	0.33	0.34	<b>0.35</b>	<b>0.35</b>
DINOv3 Web	0.82	0.84	<b>0.87</b>	<b>0.87</b>	0.36	0.36	<b>0.37</b>	<b>0.37</b>
DINOv3 Sat	0.83	0.83	<b>0.86</b>	<b>0.86</b>	<b>0.37</b>	0.36	<b>0.37</b>	<b>0.37</b>
SatlasNet	0.84	0.87	0.89	<b>0.90</b>	0.36	0.37	0.38	0.39
MPMAE	0.90	0.90	<b>0.91</b>	<b>0.91</b>	0.39	0.40	0.41	<b>0.42</b>
TerraMind	<b>0.95</b>	<b>0.95</b>	<b>0.95</b>	<b>0.95</b>	<b>0.41</b>	<b>0.41</b>	<b>0.41</b>	<b>0.41</b>
Copernicus-FM	<b>0.99</b>	<b>0.99</b>	<b>0.99</b>	<b>0.99</b>	<b>0.43</b>	<b>0.46</b>	<b>0.47</b>	<b>0.47</b>

Table S.29. Species test mAP by architecture, adaptation mode, and split (Seed 42)

Model	Random				Geographic			
	FT	JT	TTT-MMR	TTT-MMR-Geo	FT	JT	TTT-MMR	TTT-MMR-Geo
ConvNeXtV2A	0.48	0.53	0.56	<b>0.61</b>	0.32	0.32	0.34	<b>0.35</b>
Scale-MAE	0.67	0.72	<b>0.77</b>	<b>0.77</b>	0.34	0.34	<b>0.35</b>	<b>0.35</b>
DINOv3 Web	0.82	0.84	<b>0.87</b>	<b>0.87</b>	0.36	0.36	<b>0.37</b>	<b>0.37</b>
DINOv3 Sat	0.83	0.83	<b>0.86</b>	<b>0.86</b>	<b>0.37</b>	0.36	<b>0.37</b>	<b>0.37</b>
SatlasNet	0.84	0.86	0.89	<b>0.90</b>	0.36	0.37	0.38	0.39
MPMAE	0.90	0.90	<b>0.91</b>	<b>0.91</b>	0.39	0.40	0.41	<b>0.42</b>
TerraMind	<b>0.95</b>	<b>0.95</b>	<b>0.95</b>	<b>0.95</b>	<b>0.41</b>	<b>0.41</b>	<b>0.41</b>	<b>0.41</b>
Copernicus-FM	<b>0.99</b>	<b>0.99</b>	<b>0.99</b>	<b>0.99</b>	<b>0.44</b>	<b>0.47</b>	<b>0.47</b>	<b>0.47</b>

Table S.30. Species test mAP by architecture, adaptation mode, and split (Seed 43)

### S.5.3. Linear probing

The “Random” section of Tabs. S.31 to S.35 shows the numbers used to create Fig. S.11. The “100%” columns in Tabs. S.31 to S.35 were used to generate Fig. S.13. We made Fig. S.14 based off the “TerraMind S2”, “TerraMind”, “Copernicus-FM S2”, and “Copernicus-FM” rows in Tabs. S.31 to S.35. The “Geographic” section of Tabs. S.31 to S.35 shows the numbers used to create Fig. S.12.

Table S.31. Biomass linear probing test  $R^2$ 

	Random												Geographic														
	Seed 41			Seed 42			Seed 43			Seed 41			Seed 42			Seed 43			Seed 41			Seed 42			Seed 43		
	5%	50%	100%	5%	50%	100%	5%	50%	100%	5%	50%	100%	5%	50%	100%	5%	50%	100%	5%	50%	100%	5%	50%	100%	5%	50%	100%
ConvNeXtV2A	-0.34	-0.03	0.02	-0.34	-0.03	0.02	-0.34	-0.03	0.02	-0.09	-0.15	-0.10	-0.09	-0.15	-0.10	-0.09	-0.15	-0.10	-0.09	-0.15	-0.10	-0.09	-0.15	-0.10	-0.09	-0.15	-0.10
Scale-MAE	-0.33	0.04	0.09	-0.33	0.04	0.09	-0.33	0.04	0.09	-0.07	-0.05	-0.06	-0.07	-0.05	-0.06	-0.07	-0.05	-0.06	-0.07	-0.05	-0.06	-0.07	-0.05	-0.06	-0.07	-0.05	-0.06
DINOv3 Web	-0.35	0.01	0.11	-0.35	0.01	0.11	-0.35	0.01	0.11	-0.10	-0.02	-0.06	-0.10	-0.02	-0.06	-0.10	-0.02	-0.06	-0.10	-0.02	-0.06	-0.10	-0.02	-0.06	-0.10	-0.02	-0.06
DINOv3 Sat	-0.40	-0.19	-0.03	-0.40	-0.19	-0.03	-0.40	-0.19	-0.03	-0.13	-0.00	0.04	-0.13	-0.01	0.04	-0.13	-0.01	0.04	-0.13	-0.01	0.04	-0.13	-0.00	0.04	-0.13	-0.00	0.04
SatlasNet	-0.34	0.05	0.14	-0.34	0.05	0.14	-0.34	0.05	0.14	-0.09	0.02	0.02	-0.09	0.02	0.02	-0.09	0.02	0.02	-0.09	0.02	0.02	-0.09	0.02	0.02	-0.09	0.02	0.02
MPMAE	-0.29	0.10	0.19	-0.29	0.10	0.19	-0.29	0.10	0.19	-0.06	<b>0.12</b>	<b>0.21</b>															
TerraMind S2	-0.38	-0.06	0.13	-0.38	-0.06	0.13	-0.38	-0.06	0.13	-0.12	0.07	0.13	-0.12	0.07	0.13	-0.12	0.07	0.13	-0.12	0.07	0.13	-0.12	0.07	0.13	-0.12	0.07	0.13
TerraMind	-0.36	-0.00	0.13	-0.36	-0.00	0.13	-0.36	-0.00	0.13	-0.10	0.08	0.05	-0.10	0.08	0.05	-0.10	0.08	0.05	-0.10	0.08	0.05	-0.10	0.08	0.05	-0.10	0.08	0.05
Copernicus-FM S2	<b>-0.03</b>	0.12	0.13	<b>-0.03</b>	0.12	0.13	<b>-0.03</b>	0.12	0.13	-0.08	0.01	-0.02	-0.08	0.01	-0.02	-0.08	0.01	-0.02	-0.08	0.01	-0.02	-0.08	0.01	-0.02	-0.08	0.01	-0.02
Copernicus-FM	-0.09	<b>0.16</b>	<b>0.24</b>	-0.08	<b>0.16</b>	<b>0.24</b>	-0.08	<b>0.16</b>	<b>0.24</b>	<b>0.02</b>	0.08	0.19															

Table S.32. Soil nitrogen linear probing test  $R^2$ 

	Random												Geographic														
	Seed 41			Seed 42			Seed 43			Seed 41			Seed 42			Seed 43			Seed 41			Seed 42			Seed 43		
	5%	50%	100%	5%	50%	100%	5%	50%	100%	5%	50%	100%	5%	50%	100%	5%	50%	100%	5%	50%	100%	5%	50%	100%	5%	50%	100%
ConvNeXtV2A	-0.20	0.13	0.15	-0.20	0.14	0.15	-0.20	0.14	0.15	-0.20	-0.16	-0.16	-0.20	-0.16	-0.17	-0.20	-0.16	-0.17	-0.20	-0.16	-0.17	-0.20	-0.16	-0.17	-0.20	-0.16	-0.17
Scale-MAE	-0.05	0.14	0.16	-0.05	0.14	0.16	-0.05	0.14	0.16	<b>0.02</b>	-0.26	-0.25															
DINOv3 Web	0.05	0.24	0.27	0.05	0.24	0.27	0.05	0.24	0.27	-0.00	-0.33	-0.33	-0.00	-0.33	-0.33	-0.00	-0.33	-0.33	-0.00	-0.33	-0.33	-0.00	-0.33	-0.33	-0.00	-0.33	-0.32
DINOv3 Sat	0.05	0.30	0.34	0.05	0.30	0.34	0.05	0.30	0.34	-0.01	-0.10	-0.07	-0.01	-0.10	-0.07	-0.01	-0.10	-0.07	-0.01	-0.10	-0.07	-0.01	-0.10	-0.07	-0.01	-0.10	-0.07
SatlasNet	<b>0.10</b>	0.22	0.23	<b>0.10</b>	0.22	0.23	<b>0.10</b>	0.22	0.23	-0.04	-0.19	-0.17	-0.04	-0.19	-0.17	-0.04	-0.19	-0.17	-0.04	-0.19	-0.17	-0.04	-0.19	-0.17	-0.04	-0.19	-0.17
MPMAE	-0.10	0.27	0.31	-0.10	0.27	0.31	-0.10	0.28	0.31	-0.05	-0.16	-0.18	-0.05	-0.16	-0.18	-0.05	-0.16	-0.18	-0.05	-0.16	-0.18	-0.05	-0.16	-0.18	-0.05	-0.16	-0.18
TerraMind S2	-0.24	<b>0.33</b>	<b>0.41</b>	-0.24	<b>0.34</b>	<b>0.41</b>	-0.24	<b>0.34</b>	<b>0.41</b>	-0.12	<b>-0.01</b>	<b>0.03</b>															
TerraMind	-0.16	0.28	0.36	-0.16	0.28	0.36	-0.16	0.28	0.36	-0.06	-0.13	-0.04	-0.06	-0.13	-0.04	-0.06	-0.13	-0.04	-0.06	-0.13	-0.04	-0.06	-0.13	-0.04	-0.06	-0.13	
Copernicus-FM S2	-0.05	0.19	0.23	-0.05	0.19	0.23	-0.05	0.19	0.23	-0.00	-0.22	-0.26	-0.00	-0.22	-0.26	-0.00	-0.22	-0.26	-0.00	-0.22	-0.26	-0.00	-0.22	-0.26	-0.00	-0.22	-0.26
Copernicus-FM	-0.10	0.16	0.24	-0.10	0.16	0.24	-0.10	0.16	0.24	-0.00	-0.15	-0.16	-0.00	-0.15	-0.16	-0.00	-0.15	-0.16	-0.00	-0.15	-0.16	-0.00	-0.15	-0.16	-0.00	-0.15	-0.16

Table S.33. Soil organic carbon linear probing test  $R^2$ 

	Random												Geographic														
	Seed 41			Seed 42			Seed 43			Seed 41			Seed 42			Seed 43			Seed 41			Seed 42			Seed 43		
	5%	50%	100%	5%	50%	100%	5%	50%	100%	5%	50%	100%	5%	50%	100%	5%	50%	100%	5%	50%	100%	5%	50%	100%	5%	50%	100%
ConvNeXtV2A	-0.40	-0.05	0.07	-0.40	-0.05	0.07	-0.40	-0.05	0.07	-0.26	-0.37	-1.32	-0.26	-0.37	-1.32	-0.26	-0.37	-1.32	-0.26	-0.37	-1.32	-0.26	-0.37	-1.32	-0.26	-0.37	-1.32
Scale-MAE	-0.37	0.02	0.04	-0.37	0.02	0.04	-0.37	0.02	0.04	-0.17	-1.43	-1.66	-0.17	-1.43	-1.66	-0.17	-1.43	-1.66	-0.17	-1.43	-1.66	-0.17	-1.43	-1.66	-0.17	-1.43	-1.66
DINOv3 Web	<b>-0.30</b>	0.06	0.12	<b>-0.30</b>	0.06	0.12	<b>-0.30</b>	0.06	0.12	<b>-0.07</b>	-1.51	-1.83															
DINOv3 Sat	-0.33	0.08	0.15	-0.33	0.08	0.15	-0.33	0.08	0.15	-0.14	-1.11	-1.23	-0.14	-1.11	-1.23	-0.14	-1.11	-1.23	-0.14	-1.11	-1.23	-0.14	-1.11	-1.23	-0.14	-1.11	-1.23
SatlasNet	<b>-0.30</b>	<b>0.11</b>	<b>0.18</b>	<b>-0.30</b>	<b>0.11</b>	<b>0.18</b>	<b>-0.30</b>	<b>0.11</b>	<b>0.18</b>	-0.09	-1.01	<b>-0.93</b>															
MPMAE	-0.40	-0.05	0.09	-0.40	-0.05	0.09	-0.40	-0.05	0.09	-0.26	-0.11	-1.44	-0.26	-0.11	-1.44	-0.26	-0.11	-1.44	-0.26	-0.11	-1.44	-0.26	-0.11	-1.44	-0.26	-0.11	-1.44
TerraMind S2	-0.41	0.03	0.11	-0.41	0.03	0.11	-0.41	0.03	0.11	-0.28	-0.51	-1.29	-0.28	-0.51	-1.29	-0.28	-0.51	-1.29	-0.28	-0.51	-1.29	-0.28	-0.51	-1.29	-0.28	-0.51	-1.29
TerraMind	-0.40	0.05	0.09	-0.40	0.05	0.09	-0.40	0.05	0.09	-0.24	-0.87	-1.56	-0.24	-0.87	-1.56	-0.24	-0.87	-1.56	-0.24	-0.87	-1.56	-0.24	-0.87	-1.56	-0.24	-0.87	-1.56
Copernicus-FM S2	-0.37	-0.01	0.0																								

Table S.35. Species linear probing test mAP

	Random									Geographic								
	Seed 41			Seed 42			Seed 43			Seed 41			Seed 42			Seed 43		
	5%	50%	100%	5%	50%	100%	5%	50%	100%	5%	50%	100%	5%	50%	100%	5%	50%	100%
ConvNeXtV2A	0.32	0.34	0.35	0.32	0.34	0.35	0.32	0.34	0.35	0.28	0.29	0.29	0.28	0.29	0.29	0.28	0.29	0.29
Scale-MAE	0.37	0.48	0.50	0.37	0.48	0.50	0.37	0.48	0.50	0.28	0.31	0.32	0.28	0.31	0.32	0.28	0.31	0.32
DINOv3 Web	0.46	0.59	0.62	0.46	0.59	0.62	0.46	0.59	0.62	0.33	0.36	0.36	0.33	0.36	0.36	0.33	0.36	0.36
DINOv3 Sat	0.52	0.68	0.71	0.52	0.68	0.71	0.52	0.68	0.71	0.33	0.37	0.37	0.33	0.37	0.37	0.33	0.37	0.37
SatlasNet	0.43	0.55	0.57	0.43	0.55	0.57	0.43	0.55	0.57	0.32	0.33	0.34	0.32	0.33	0.34	0.32	0.33	0.34
MPMAE	0.45	0.67	0.70	0.45	0.67	0.70	0.45	0.67	0.70	0.30	0.36	0.36	0.30	0.36	0.36	0.30	0.36	0.36
TerraMind S2	<b>0.66</b>	<b>0.85</b>	<b>0.87</b>	<b>0.65</b>	<b>0.85</b>	<b>0.87</b>	<b>0.66</b>	<b>0.85</b>	<b>0.87</b>	<b>0.39</b>	<b>0.43</b>	<b>0.43</b>	<b>0.39</b>	<b>0.43</b>	<b>0.43</b>	<b>0.43</b>	<b>0.43</b>	<b>0.43</b>
TerraMind	0.58	0.82	0.86	0.58	0.82	0.86	0.58	0.82	0.86	0.35	0.42	0.42	0.35	0.42	0.42	0.35	0.42	0.42
Copernicus-FM S2	0.38	0.53	0.57	0.38	0.53	0.57	0.38	0.53	0.57	0.29	0.31	0.32	0.29	0.31	0.32	0.29	0.31	0.32
Copernicus-FM	0.44	0.70	0.78	0.44	0.70	0.78	0.44	0.70	0.78	0.31	0.40	<b>0.43</b>	0.31	0.40	<b>0.43</b>	0.31	0.40	<b>0.43</b>

## S.6. Larger figures

For printing purposes, we provide larger versions of the results figures in the main paper in Figs. [S.17](#) to [S.20](#).

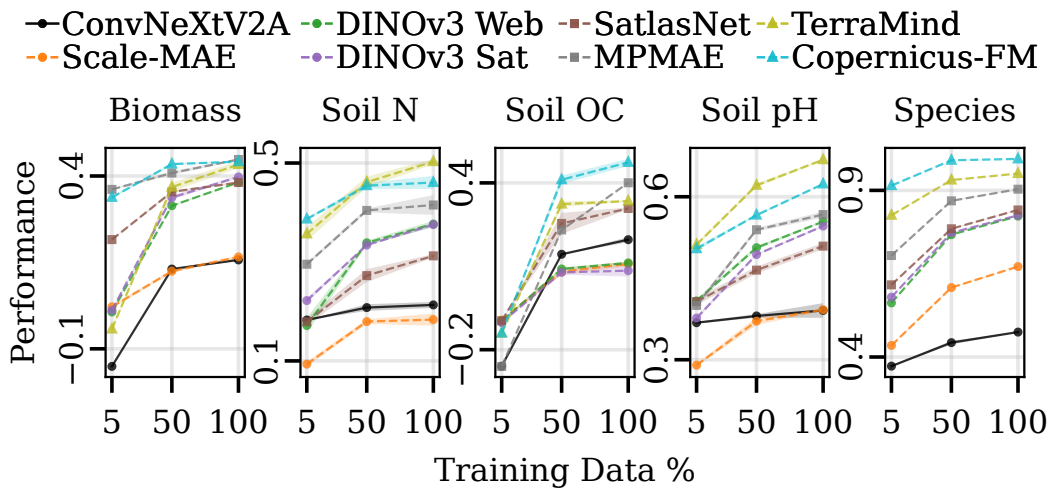


Figure S.17. Enlarged Figure 4.

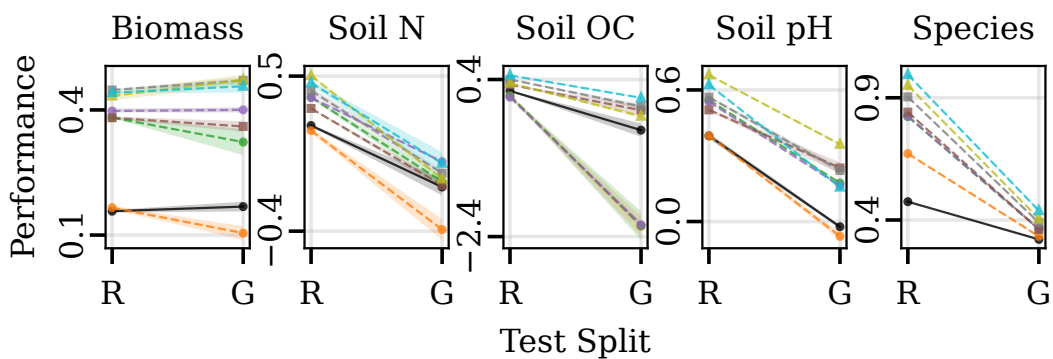


Figure S.18. Enlarged Figure 5.

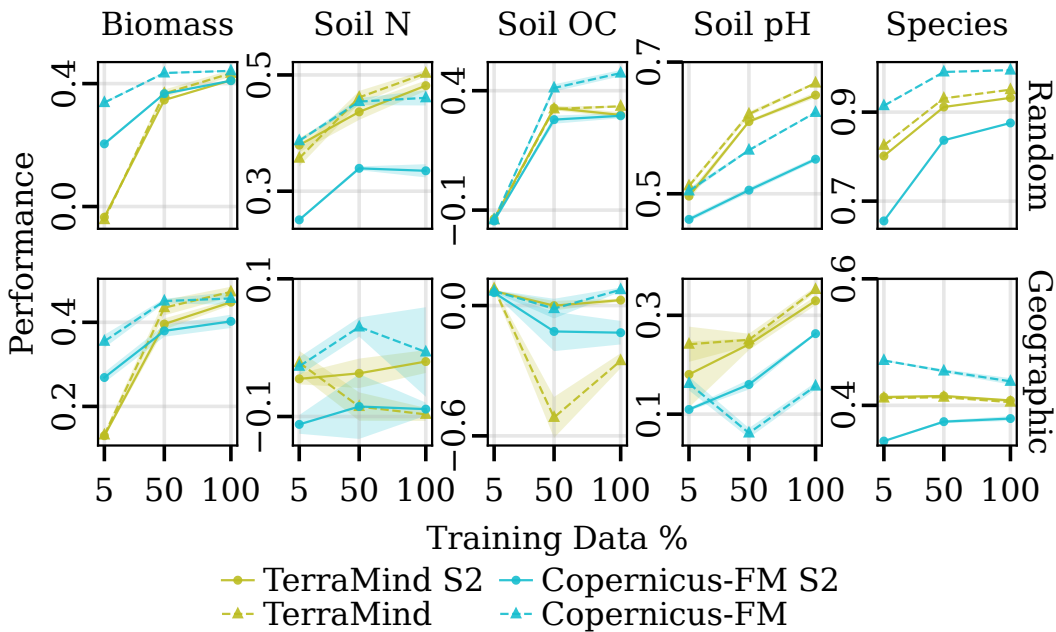


Figure S.19. Enlarged Figure 6.

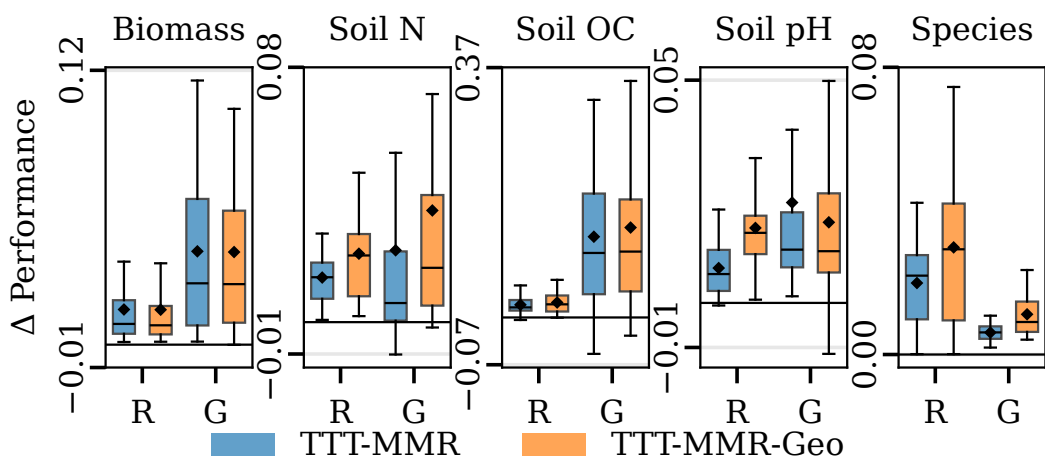


Figure S.20. Enlarged Figure 7.